The thermodynamics of rare earth element liberation, mobilization and supergene enrichment during groundwater-regolith interaction

Martin Yan Hei Li[1], Hiu Tung Kwong[1], Anthony E. Williams-Jones[1, 2], Mei-Fu Zhou[1*]

1 Department of Earth Sciences, The University of Hong Kong, Pokfulam Road, Hong Kong

2 Department of Earth and Planetary Sciences, McGill University, Montréal, Québec H3A 0E8, Canada

---

*Corresponding author:

Mei-Fu Zhou

Email: mfzhou@hku.hk

Li, M. Y. H., Kwong, H. T., Williams-Jones, A. E., and Zhou, M.-F., 2021,
The thermodynamics of rare earth element liberation, mobilization and supergene enrichment during groundwater-regolith interaction: Geochimica et Cosmochimica Acta.

Abstract

Rare earth elements (REEs) mobilize, fractionate, and are re-distributed during supergene processes, and thus provide a powerful tool with which to quantitatively reconstruct the effects of chemical weathering. Some of the key processes controlling the behavior of the REEs during chemical weathering, notably the dissolution of REE minerals, and the relative mobility of individual REE during the interaction of groundwaters with the regolith, however, are poorly understood. Nonetheless, it is well-known that, under certain conditions, the REEs can concentrate to levels in the regolith sufficient to form giant REE deposits. It is also well-known, that these deposits are responsible for much of the World's production of heavy REEs (HREEs). As the REEs, and particularly the HREEs, have become economically critical because of their role as essential elements for technologies required to create a carbon neutral global society, there is now a pressing need to find new resources of these metals. Understanding the supergene behavior of the REEs is an important first step towards meeting this need.

Thermodynamic calculations predict that dissolution of the main REE minerals in REE-rich protoliths, namely synchysite-(Y), gadolinite-(Y), hingganite-(Y), yttrialite-(Y), allanite-(Ce), titanite, eudialyte, chevkinite-(Ce), and loparite-(Ce), should occur spontaneously during weathering. It therefore follows that a high abundance of these minerals in the protolith implies high mobility of the REE during weathering and consequently a high potential for the discovery of economic REE resources. Dissolution of apatite, monazite, and synchysite-(Ce) is promoted strongly by metamictization or structural distortion and could be also important at low pH. In contrast, some LREE-fluorocarbonate minerals, notably bastnäsite-(Ce) and parisite-(Ce), are thermodynamically stable in acidic environments. Thus, they would be preserved in the regolith. Zircon, fergusonite, and xenotime are resistant to acidic dissolution, consistent with their common occurrence as residual minerals.

Li, M. Y. H., Kwong, H. T., Williams-Jones, A. E., and Zhou, M.-F., 2021,
The thermodynamics of rare earth element liberation, mobilization and supergene enrichment during groundwater-regolith interaction: Geochimica et Cosmochimica Acta.

In the case of the world-class regolith-hosted REE deposits in South China, the groundwater is mildly acidic to circum-neutral and carbonate-rich. The REEs are consequently transported dominantly as hydrated cations and carbonate complexes, depending on the pH. The proportion of the Y-species (simple ion or carbonate complex) varies either positively or negatively in relation to Ho and Er, the adjacent lanthanides with similar ionic radii, depending on the pH and carbonate concentration of the regolith water and, significantly, the inverse of this geochemical signature is inherited by the clay-sorbed fraction of the REEs in the regolith. A similar phenomenon is observed for Sm, Gd, and Yb. This indicates that the REEs are scavenged from the regolith water by the clay minerals in the regolith. Among these clay minerals, halloysite has the greatest capacity to adsorb and retain the HREEs, likely through surface complexation or incorporation at interlayer sites, depending on the pH and carbonate concentration of the water, and is the strongest contributor to the HREE-rich regolith. Mixing of the regolith water with the alkaline and carbonate-rich aquifer groundwater increases the pH and carbonate concentration and, in turn, affects the ability of the mixed water to transport the HREEs. The juxtaposition of a HREE-bearing weathering fluid and halloysite in the regolith results in the efficient accumulation of the HREEs in the latter and has led to the formation of the world-class regolith-hosted deposits that now meet much of the global need for the HREEs.

Li, M. Y. H., Kwong, H. T., Williams-Jones, A. E., and Zhou, M.-F., 2021,
The thermodynamics of rare earth element liberation, mobilization and supergene enrichment during groundwater-regolith interaction:
Geochimica et Cosmochimica Acta.

1. Introduction

The rare earth elements (REEs), namely the lanthanide group elements, plus yttrium (Y) and scandium (Sc), can be divided into light REEs (LREEs) and heavy REEs (HREEs). Apart from Sc, these elements show similar geochemical behavior, but fractionate strongly in some geological environments. Such characteristics make them powerful proxies with which to trace a variety of processes in the Earth system. Moreover, these elements, especially the HREEs, have become increasingly important economically, as they are essential components in a variety of high-technology applications, including many that are being implemented to address issues of global warming. Enrichment of the REEs to form economic deposits occurs naturally in environments ranging from those of magmatic-hydrothermal systems to ambient temperature chemical weathering (Smith et al., 2016; Williams-Jones et al., 2012), with the latter being particularly important for the HREEs, which dominate the global supply of these elements through their production from regolith-hosted deposits .

During weathering, the REEs are mobilized by the dissolution of REE-bearing minerals, the nature of which varies depending on the protolith. In the case of granites and other felsic igneous rock-types that are enriched in the REEs relative to other igneous rock-types (and their sedimentary equivalents), these minerals are mainly monazite, xenotime, apatite, allanite, titanite, and zircon (Emsbo et al., 2016; Hoskin et al., 2000; Li et al., 2017). The REEs, however, reach their highest concentrations in carbonatites, phoscorites and alkaline complexes, and these rocks types, although relatively uncommon, can be important protoliths for the formation of supergene REE deposits, such as the Mt Weld deposit in Australia (Lottermoser, 1990). In these rock-types, fluorocarbonates, such as bastnasite-(Ce) and parisite-(Ce), loparite-(Ce), niobates, and eudialyte could be important REE hosts, in addition to the minerals mentioned above (Möller and Williams-Jones, 2017; Sheard et al., 2012; Vasyukova and Williams-Jones, 2020; Verplanck et al., 2016; Verplanck and Van Gosen, 2011). Recently, we showed that

Li, M. Y. H., Kwong, H. T., Williams-Jones, A. E., and Zhou, M.-F., 2021,
The thermodynamics of rare earth element liberation, mobilization and supergene enrichment during groundwater-regolith interaction: Geochimica et Cosmochimica Acta.

synchysite-(Y), gadolinite-(Y), and hingganite-(Y) can be important sources of the HREE in granites (Li et al., 2019). Unfortunately, the stability of many of the minerals mentioned above in aqueous fluids has not been determined experimentally or theoretically, even for ambient temperature. As REE mineral dissolution is a major determinant for the supergene enrichment of the REEs, understanding their dissolution is an essential precondition for modeling the formation of economic regolith-hosted REE and particularly HREE deposits.

In contrast to the paucity of information on REE mineral dissolution, a relatively large body of knowledge has accumulated on the aqueous complexation of the REE and their mobilization, particularly at ambient temperature (e.g., Haas et al., 1995; Johannesson et al., 1999; Johannesson et al., 1996; Johannesson et al., 2000; Luo and Byrne, 2004; Wood, 1990). Moreover, numerous studies have documented the fractionation of the LREEs from the HREEs during weathering. Interestingly, the regolith is commonly depleted in the HREEs relative to the LREEs with progressive weathering (e.g. Aubert et al., 2001; Braun et al., 1993; Braun et al., 1998; da Silva et al., 2017; Nesbitt, 1979; Yusoff et al., 2013). This is probably because HREEs form considerably stronger complexes with CO_3^{2-} than the LREEs at ambient temperature (Luo and Byrne, 2004), especially in circum-neutral and alkaline groundwater (Johannesson et al., 1999; Johannesson et al., 1996; Johannesson et al., 2000). The HREEs are therefore, more efficiently removed from the regolith than the LREEs, ending up in groundwater, river water and seawater (Aubert et al., 2001; Braun et al., 1998; Elderfield et al., 1990; Tang and Johannesson, 2010; Wood, 1990). This suggests that significant HREE accumulation should not occur during weathering, which raises the question of why in some cases, notably in the giant regolith-hosted deposits, there is economic enrichment of HREEs (Li et al., 2019). Possible reasons for the apparent contradiction could be differences in the nature of the protolith REE mineralogy, the supergene mineralogy and the aqueous REE

Li, M. Y. H., Kwong, H. T., Williams-Jones, A. E., and Zhou, M.-F., 2021,
The thermodynamics of rare earth element liberation, mobilization and supergene enrichment during groundwater-regolith interaction:
Geochimica et Cosmochimica Acta.

complexation (Laveuf and Cornu, 2009), all of which could lead to considerable differences in the behavior of the individual REEs.

In this study, we use two deposits REE deposits in South China that have been investigated by us (Li et al., 2019, 2020) to evaluate REE mineral dissolution and REE mobilization during weathering, from a thermodynamic perspective. Building on this evaluation, we examine the role of groundwater-regolith interaction in the supergene REE enrichment process and the formation of world-class regolith-hosted deposits.

2. Deposit geology

Nearly all of the regolith-hosted REE deposits that are currently being exploited are located in South China (Li et al., 2017; Sanematsu and Watanabe, 2016). Among these deposits, the Zudong HREE deposit, which is one of the subjects of this study, is the largest with an approximate resource of 18,000 t REO (Fig. 1). Generally, the ore bodies vary from a few meters to 20 m in thickness. They are found near the pedolith-saprolite interface of the weathering crusts and are situated on a moderately undulating surface with slope gradients between 10° and 15° (Li et al., 2019). Kaolinite and halloysite are the dominant clay minerals (>90% of the clay-sized fraction in the ore zone) in the soil profiles, i.e., in both the pedolith and saprolite (Li and Zhou, 2020). Minor proportions of illite and smectite are present in the lower saprolite. Supergene REE minerals, notably chernovite-(Y), and residual REE-bearing minerals, including zircon, xenotime-(Y), and euxenite-(Y), are common in the soil profiles. The protolith to the Zudong deposit is a late Jurassic, HREE-rich granite, composed of quartz, K-feldspar, albite, and muscovite with most of the REEs being hosted in accessory minerals, including synchysite-(Y), gadolinite-(Y), hingganite-(Y), yttrialite-(Y), xenotime-(Y), REE niobates, yttrian fluorite, and zircon (Fig. 2). Synchysite-(Y), gadolinite-(Y), hingganite-(Y), and, yttrialite-(Y) are interpreted to be hydrothermal in origin, based on their occurrence in

Li, M. Y. H., Kwong, H. T., Williams-Jones, A. E., and Zhou, M.-F., 2021,
The thermodynamics of rare earth element liberation, mobilization and supergene enrichment during groundwater-regolith interaction:
Geochimica et Cosmochimica Acta.

veinlets and as laths replacing feldspars and micas (Fig. 2c) (Li et al., 2019). Owing to their rare appearance in the regolith, these minerals are thought to be very susceptible to weathering and to have supplied most of the HREEs to the fluids that concentrated them in the deposit (Li et al., 2019).

The other deposit on which this study based is the Bankeng deposit, a LREE-dominant deposit adjacent to the Zudong deposit (Fig. 1). This deposit is currently being explored and has grades between 0.1 wt.% and 0.13 wt.%. REO. The deposit is located along the ridges of gently undulating catchments with slope gradients varying between 15 and 20º. The soil profiles vary between 1 m and ~10 m in thickness. Although the REE enrichment is greatest at the ridgetops, it is noteworthy that the more weakly REE enriched footslope is characterized by preferential HREE enrichment (Li et al., 2020). As is the case for the Zudong deposit, kaolinite and halloysite are the principal clay minerals (~70% of the clay-sized fraction in the ore zone) and are accompanied by minor vermiculite, illite and smectite. The main supergene REE minerals are rhabdophane-(Ce) and cerianite-(Ce), which are found mainly in the saprolite and pedolith, respectively. Residual zircon, monazite, and thorite are also commonly observed in the soil profiles. The protolith for the Bankeng deposit is a late Triassic granite composed of quartz, K-feldspar, albite, biotite, and chlorite. The REEs are mostly hosted in accessory monazite (Fig. 3a & b), apatite (Fig. 3b & d), bastnäsite-(Ce) and parisite-(Ce) (Fig. 3c). As apatite, and REE-fluorocarbonates are not observed in the saprolite, it seems likely that they were the source of the REE supplied to the fluids that formed the deposit (Li et al., 2020).

3. Materials and methods

3.1 Evaluation of mineral stability during weathering

3.1.1 Gibbs free energy of formation

Li, M. Y. H., Kwong, H. T., Williams-Jones, A. E., and Zhou, M.-F., 2021,
The thermodynamics of rare earth element liberation, mobilization and supergene enrichment during groundwater-regolith interaction:
Geochimica et Cosmochimica Acta.

The first step in evaluating the stability of REE minerals during weathering was to establish their Gibbs free energy of formation. In addition to the REE minerals observed in the Zudong and Bankeng deposits, we also considered REE minerals commonly observed in granites, rhyolites, carbonatites, phoscorites, alkaline rocks, and metapelites. The latter minerals include allanite-(Ce) (Fig. 3e), titanite (Fig. 3f), eudialyte, chevkinite-(Ce), fergusonite-(La), and loparite-(Ce).

In the case of minerals for which the Gibbs free energy of formation (G_f) has not been determined experimentally, notably gadolinite-(Y), hingganite-(Y), yttrialite-(Y), allanite-(Ce), eudialyte, chevkinite-(Ce) and loparite-(Ce), we employed the polyhedral approach for estimation (Chermak and Rimstidt, 1989; Hazen, 1988). In this approach, the G_f of a mineral is estimated by assuming that the mineral is composed of a set of basic polyhedral units. The G_f of the mineral of interest is thus the sum of the molar Gibbs free energy of formation (g_i) of the individual polyhedral units:

Gadolinite-(Y): $Y_2FeBe_2Si_2O_{10} = Y_2O_3 + Fe^{(II)}O + 2BeO + 2SiO_2$

Hingganite-(Y): $Y_2Be_2(SiO_4)_2(OH)_2 = Y_2O_3 + 2BeO + 2SiO_2 + H_2O$

Yttrialite-(Y): $Y_2Si_2O_7 = Y_2O_3 + 2SiO_2$

Allanite-(Ce): $CaCeAl_2Fe^{II}(SiO_4)_3(OH) =$

$CaO + 0.5Ce_2O_3 + Al_2O_3 + FeO + 3SiO_2 + 0.5H_2O$

Eudialyte: $Na_{15}Ca_6Fe^{II}_3Zr_3Si(Si_{25}O_{72})(OH)_5 =$

$7.5Na_2O + 6CaO + 3FeO + 3ZrO_2 + 26SiO_2 + 2.5H_2O$

Chevkinite-(Ce): $Ce_4Fe^{II}Fe^{III}_2Ti_2(Si_2O_7)_8 = 2Ce_2O_3 + FeO + Fe_2O_3 + 2TiO_2 + 4SiO_2$

Loparite-(Ce): $(Na,Ce)(Nb,Fe^{III})O_6 = 0.5Na_2O + 0.5Ce_2O_3 + 0.5Nb_2O_5 + 0.5Fe_2O_3$

The values of g_i for the polyhedral units used in the calculation were compiled from the literature and are reported in Table S1. As the Gibbs free energy of formation of the TiO_2 and BeO polyhedral components are not available from the literature, their g_i values were calculated

Li, M. Y. H., Kwong, H. T., Williams-Jones, A. E., and Zhou, M.-F., 2021,
The thermodynamics of rare earth element liberation, mobilization and supergene enrichment during groundwater-regolith interaction: Geochimica et Cosmochimica Acta.

using the relationship: $g_i = h_i - Ts_i$, with values for h_i and s_i taken from Van Hinsberg et al. (2005) of -955.507 ± 35.677 KJ mol^{-1} and 55.4 ± 6.03 J mol^{-1} K^{-1}, and -609.161 ± 3.516 KJ mol^{-1} and 11.8 ± 0.68 J mol^{-1} K^{-1}, respectively. In this relationship *hi* and s_i are the molar enthalpy of formation and molar standard entropy, respectively. As the standard deviations (SD) of the molar Gibbs free energy of formation (g_i) of the TiO_2 and BeO polyhedral units are not known, they were assumed to be 5%; the SD for the g_i of the other polyhedral units are all reported to be <5%.

The G_f of fergusonite-(La) was calculated using the relationship: $G_f = H_f - TS_f$, and values of H_f and S_f of -1924.3 KJ mol^{-1} (Reznitskii, 2001) and 128.99 ± 0.28 J mol^{-1} K^{-1} (Nikiforova et al., 2019), respectively. As values for the enthalpy and entropy of formation of fergusonite-(Y) have not been reported, they were estimated from the corresponding data for other niobates. The H_f value was estimated by interpolating the experimentally determined H_f for a set of other REE niobates (Reznitskii, 2001) against the 8-fold coordinated radii of the corresponding REEs (Shannon, 1976). The value for S_f was estimated by extrapolating experimentally determined S_f values for $LaNbO_4$ and $GdNbO_4$ (Kondrat'eva et al., 2019; Nikiforova et al., 2019) against the corresponding 8-fold coordinated radii of La and Gd, respectively (Shannon, 1976). The estimated values for H_f and S_f were then used to estimate the G_f of fergusonite-(Y) using the relationship: $G_f = H_f - TS_f$.

The thermodynamic properties of the REE-fluorocarbonates, bastnäsite-(Ce) and parisite-(Ce) have been determined experimentally (Gysi and Williams-Jones, 2015) and the G_f of bastnäsite (Ce, La, Nd and Pr) has been estimated by a combination of methods by (Al-Nafai et al., 2019). We estimated the G_f for the other REE endmembers of these phases by interpolating their G_f values from the relationship of the known values to the ionic radii of the corresponding REE in 9-fold coordination (Shannon, 1976). The G_f of the various synchysite

Li, M. Y. H., Kwong, H. T., Williams-Jones, A. E., and Zhou, M.-F., 2021,
The thermodynamics of rare earth element liberation, mobilization and supergene enrichment during groundwater-regolith interaction:
Geochimica et Cosmochimica Acta.

endmembers was estimated assuming G_f corresponds to the sum of the g_i of the corresponding bastnäsite, a CaO and a CO_2 unit.

In Table S2, we report the G_f of the minerals discussed above as well as the G_f of the other minerals used in calculating the ΔG of the dissolution reactions (ΔG_r) at ambient conditions discussed below. The standard deviations (SD) of the Gibbs free energy of formation (G_f) of minerals for which the SD has not been evaluated, were considered to be 1% of the corresponding G_f, as the SD of the G_f of the other minerals are all <1% of the value of this parameter.

3.1.2 Calculation of equilibrium constants and reaction quotients

The spontaneity of parental REE mineral dissolution was evaluated from the solubility products (Ksp) for the different REE minerals, the equilibrium constants (K) for dissolution reactions that take into account the speciation of the aqueous solvent and the reaction quotient (Q). Values of Ksp and K at 298 K and saturated vapor pressure were calculated using the Unitherm program in the HCh software package (Shvarov, 1999). The reaction quotients (Q) were calculated using the activity of the relevant chemical species in the regolith water and groundwater (Table 1 and 2). As the water analyses for Zudong do not contain data on the concentrations of Si, P, Zr, Nb, and Be (see sections 3.2.1 and 3.2.2), the concentrations of these elements were assumed to be the same as those in the water sampled at Bankeng. Considering that the two sites are adjacent to each other, the concentrations of these elements probably does not vary significantly. Also, for simplicity, the activity of Y^{3+} and Ce^{3+} or La^{3+} for fergusonite (YCO_3^+, $CeCO_3^+$, and $LaCO_3^+$ for the reactions involving bicarbonate ion) were adopted to represent the REE^{3+} from the HREE- and LREE-bearing minerals ,respectively. The activity of the various chemical species was calculated using the PHREEQC program (See sections 3.1.1 and 3.2.2 for determination of elemental compositions and the activity of species

Li, M. Y. H., Kwong, H. T., Williams-Jones, A. E., and Zhou, M.-F., 2021,
The thermodynamics of rare earth element liberation, mobilization and supergene enrichment during groundwater-regolith interaction:
Geochimica et Cosmochimica Acta.

in the water samples). Two reaction pathways, one representing a more acidic environment, (Table 1) and the other (Table 2), representing a more alkaline environment, involving the bicarbonate ion, were considered.

3.2 Evaluation of aqueous REE speciation

3.2.1 Sampling, pH and alkalinity measurement

Water samples from the Bankeng deposit were collected at a depth of 5.5 m at the foot-slope of an ore-bearing catchment (corresponding to the saprolite zone of the soil profile). The depth to the top of the water table was measured and samples collected from a standpipe installed after rotary drilling. Water was pumped out manually for 5 minutes and discarded before sample collection. The samples collected were filtered (φ = 0.22 μm) in the field and the pH and alkalinity were measured immediately. The pH was measured with a calibrated Thermo Fisher refillable AgCl electrode (Model: 9156BNWP) having an uncertainty of ±0.01. The phenolphthalein total alkalinity was measured using the HACH Method 8203 (HACH, 2018), which involved the use of Bromcresol green-methyl red and phenolphthalein indicator powder and sulfuric acid (0.16 N). As the phenolphthalein alkalinity was consistently zero, the HCO_3^- concentration was determined from the total alkalinity as follows:

$$\text{Alkalinity as } HCO_3^- \text{ (mg/L)} = 1.22 \times \text{Alkalinity as } CaCO_3 \text{ (meq/L)};$$

where bicarbonate alkalinity = total alkalinity, if the phenolphthalein alkalinity = 0. The remaining samples were acidified and stored in acid-cleaned polyethylene bottles under refrigeration at 4°C.

Owing to prolonged *in-situ* mining with chemical leaching, it is now, unfortunately, not possible to sample uncontaminated water from the Zudong deposit. Compositional data for the regolith and aquifer groundwater are, however, available from Wu (1988). The regolith water was sampled from exploration pits prior to mining activity but as the water table at that time

Li, M. Y. H., Kwong, H. T., Williams-Jones, A. E., and Zhou, M.-F., 2021,
The thermodynamics of rare earth element liberation, mobilization and supergene enrichment during groundwater-regolith interaction:
Geochimica et Cosmochimica Acta.

fluctuated around the pedolith-saprolite interface, indicating that there was interaction of the regolith water with the ore bodies the groundwater was sampled from a drill hole at a depth of 148 m (Wu, 1988). Water from this well is considered to be representative of the deep-circulating groundwater present in the vicinity of both the Zudong and Bankeng deposits.

3.2.2 Major ion, TOC and REE concentration measurement

The concentrations of major ions in the water samples collected from the Bankeng deposit were measured by ion chromatography (Thermo Scientific Dionex ICS-1100). The equipment had been calibrated with Dionex Six Cation-II and Dionex Seven Anion Standards with three injections of the original standards and standards freshly prepared by two-, three-, five- and ten-fold dilutions. The analytical errors were <10%. The total organic carbon (TOC) content was measured with a Shimadzu TOC-L TOC analyzer at the Hong Kong Baptist University. Rare earth element concentrations were analyzed with an Agilent 7900 ICP-MS at the University of Hong Kong with rhodium as an internal standard. Analysis of each sample was blanketed by two analyses of the blank solutions in 2% HNO_3 (trace metal grade) to improve accuracy. Calibration lines were constructed with multi-element standard solutions MISA-01-1, -04-1, -05-1, and -06-1 (AccuStandard). Detection limits for the different elements were determined using the blank solutions. Both the accuracy and precision errors were <10%.

The groundwater composition for the Zudong deposit was taken from the study by Wu (1988). Concentrations of major ions and the REEs were determined using ICP-AES and catalytic current polarography, respectively. Analytical errors were not reported. By assuming that there are no elemental anomalies for the HREEs (from Gd to Tm; except Y) in the groundwater and normalizing the REE profile reported in Wu (1988) (Fig. 4a) to a best-fit line for these HREEs, the analytical error for the REE concentration is estimated to be ~50%.

Li, M. Y. H., Kwong, H. T., Williams-Jones, A. E., and Zhou, M.-F., 2021,
The thermodynamics of rare earth element liberation, mobilization and supergene enrichment during groundwater-regolith interaction:
Geochimica et Cosmochimica Acta.

3.2.2 Speciation determination

The aqueous speciation at 25°C was calculated using the PHREEQC program (Parkhurst and Appelo, 2013). Activity coefficients were calculated using the extended Debye-Hückel equation, valid for ionic strengths (I) <0.1 M (Maximum I is 0.012 M for the analyzed samples; Table 2). The following REE species were considered $REECO_3^+$, $REE(CO3)_2^-$, $REEHCO_3^{2+}$, $REE(OH)^{2+}$, $REE(OH_2)^+$, $REE(OH)_3$, $REEF^{2+}$, $REEF_2^+$, $REECl^{2+}$, $REESO_4^+$, and $REENO_3^{2+}$, the infinite dilution stability constants and sources of which are reported in Table S3. An ionic strength correction was not made for the stability constants considering the dilute nature of the samples. As the pH of the regolith water from Zudong varies between 5.4 and 6 (See Results for details), we adopted these two pH values as the upper and lower boundaries for the speciation calculation. A sensitivity check was performed for the REE speciation using a second set of stability constants for $REECO_3^+$ and $REE(CO3)_2^-$, as carbonate complexes are expected to be the major species in the water samples (See Table S3 for the data source). The error of estimation of the calculated concentration of the species in the Bankeng groundwater is estimated to be ~10%. Calculated saturation indices for the minerals are provided in Table S4.

4. Results

4.1 Relative stability of REE minerals during weathering

The logarithms of the solubility products (log Ksp) of the principal minerals in the Zudong granite deemed to be the source of the HREE in the regolith, namely synchysite-(Y), gadolinite-(Y), hingganite-(Y), and yttrialite-(Y), are all positive at 25 °C, indicating that these minerals should dissolve spontaneously in water at ambient conditions (Table 1). The other HREE-bearing minerals in the Zudong granite, i.e., xenotime-(Y) fergusonite-(Y) and zircon, have negative values of log Ksp implying that their dissolution is not favored; they are common

detrital minerals in the regolith, consistent with their predicted insolubility. Some common LREE minerals, e.g., monazite-(Ce) and the LREE-fluorocarbonates and the REE-bearing mineral, apatite also have negative log Ksp values, whereas others, e.g., allanite-(Ce), titanite, eudialyte, chevkinite-(Ce), and loparite-(Ce) have positive values of log Ksp, indicating that they would likely dissolve. It is thus noteworthy that the LREE-fluorocarbonates and apatite are thought to be the source of the LREE in the Bankeng regolith because of their presence in the granite but absence from the regolith. This issue is addressed further in the discussion (Section 5.1.1)

4.2 Groundwater chemistry

The aquifer groundwater in the Zudong district is alkaline (pH = 8.5) and has an ionic strength of 0.012 M. It is dominated by HCO_3^- (~570 mg/L) and contains significant proportions of CO_3^{2-} (~20 mg/L) and SO_4^{2-} (~30 mg/L). There are also high concentrations of Cl^- (~10 mg/L) and F^- (~5 mg/L). Sodium is the dominant cation (~220 mg/L). In contrast to the groundwater, the regolith water is slightly acidic (pH = 5.4 - 6) and dilute (I = 0.001 M). It contains much less HCO_3^- (~30 mg/L), although this is the dominant anionic species, followed by Cl^- (~3 mg/L), SO_4^{2-} (~1.5 mg/L), and F^- (~0.5 mg/L) (Table 3). Concentrations of major cations, such as Na and K, in the regolith groundwater are also much lower than those in the aquifer groundwater. On the other hand, both the aquifer and regolith water have similar REE concentrations of ~5 µg/L and are HREE-enriched. Both also display significant negative Ce and Eu anomalies and a slightly positive Y anomaly (Fig. 4).

Regolith water collected from the Bankeng deposit is nearly neutral (pH = ~7.4) and has an average ionic strength of 0.008 M. It is HCO_3^--rich (~150 mg/L) and also contains considerable amounts of SO_4^{2-} (~45 mg/L), NO_3^- (~50 mg/L), and Cl^- (~22 mg/L), as well as a minor amount of F^- (~0.2 mg/L). The dominant cation is Ca^{2+} (~70 mg/L), followed by K^+ (~35

Li, M. Y. H., Kwong, H. T., Williams-Jones, A. E., and Zhou, M.-F., 2021,
The thermodynamics of rare earth element liberation, mobilization and supergene enrichment during groundwater-regolith interaction: Geochimica et Cosmochimica Acta.

335 mg/L), Na^+ (~20 mg/L), and Mg^{2+} (~10 mg/L). The TOC content is ~1.5 mg/L. The REE
336 concentrations are ~9 µg/L and include a HREE enrichment (Table 3). Like Zudong, the
337 regolith water at Bankeng exhibits negative Ce and positive Y anomalies but, instead, the Eu
338 anomaly is slightly positive (Fig. 4).
339
340 **4.3 Inorganic aqueous REE speciation**
341 More than 90% of the REE in the groundwater of the Zudong deposit is interpreted to
342 be dissolved as $REE(CO_3)_2^-$ and the proportion of this species increases progressively across
343 the lanthanide series. The only other significant species is $REECO_3^+$ and its proportion is
344 interpreted to decrease with increasing atomic number of the lanthanides (Fig. 5a).
345 In the regolith water at Zudong, the LREEs occur mainly as REE^{3+} and to a much
346 smaller extent as $REECO_3^+$, the proportion of which generally increases with increasing atomic
347 number of the REEs (Fig. 5b). Interestingly, Sm and Y behave differently from the REEs
348 closest in atomic number to them, i.e., the proportion of $SmCO_3^+$ is anomously high and the
349 proportion of YCO_3^+ is anomalously low. Other species, such as $REEHCO_3^{2+}$, $REESO_4^+$, and
350 $REEF^{2+}$, make up <10% of the dissolved REE budget. The charge imbalance in the regolith
351 water of the Zudong deposit is ~30% (Table 1), which probably reflects the low accuracy of
352 analyses in the late 1980s, when the data were obtained. In order to compensate for the excess
353 in anions, the speciation calculation was also performed by lowering the HCO_3^- concentrations
354 in the regolith groundwater to 25, 20, 15, and 10 mg/L (corresponding to a charge imbalance
355 of ~5%), respectively. The result was an increase in the proportions of REE^{3+} and a decrease
356 in the proportions of $REECO_3^+$ with HCO_3^- concentration. Nonetheless, the general distribution
357 across the lanthanides remained the same and the concentrations of Sm and Y are still
358 anomalous (Fig. 5c - f). The same result was obtained with a sensitivity check using another
359 set of stability constants, except that the proportions of the carbonate species are higher (Fig.

Li, M. Y. H., Kwong, H. T., Williams-Jones, A. E., and Zhou, M.-F., 2021,
The thermodynamics of rare earth element liberation, mobilization and supergene enrichment during groundwater-regolith interaction:
Geochimica et Cosmochimica Acta.

S1 and S2). As the accuracy with which the REE concentrations in the Zudong groundwater were analyzed, is likely to have been low, we have more confidence in the relative proportions of the different REE species because all the REE would have been subjected to a similar degree of uncertainty. Thus, it is the shapes of the profiles shown in Fig. 5 and not the abundances of the individual REE species that is important.

Regolith water in the Bankeng deposit is dominated by the carbonate and bicarbonate species (Fig. 6) and the proportions of $REECO_3^+$ and $REE(CO_3)_2^-$ generally decrease and increase across the lanthanides, respectively. The other interesting observation is that the proportions of $REECO_3^+$ complexes for Gd, Y, and Yb are anomalously high with respect to their neighboring REEs, whereas the corresponding proportions of $REE(CO_3)_2^-$ complexes for these elements are anomalously low. Proportions of the other species are all very low.

5. Discussion

5.1 REE behavior during groundwater-regolith interaction

5.1.1 Dissolution of REE minerals

The solubility product (discussed in section 4.1) provides an indication of whether a mineral is likely to dissolve in water or resist dissolution, however, mineral dissolution is also dependent on the composition of the fluid and its speciation. The latter were taken into account by replacing the reactions governing the solubility product with reactions that reflect this speciation, and the use of the reaction quotient (Q), which is the ratio of the multiples of the activity of the product to reactant species in the solution. Values of log Q that are less than the values of log K for the corresponding reactions imply that the minerals are unstable and, ignoring kinetic inhibitions, should dissolve spontaneously. In the case of Zudong, synchysite-(Y), gadolinite-(Y), hingganite-(Y) and yttrialite-(Y), which are considered to be the source of the HREE because of their common occurrence in the granite and absence in the regolith (Li

Li, M. Y. H., Kwong, H. T., Williams-Jones, A. E., and Zhou, M.-F., 2021,
The thermodynamics of rare earth element liberation, mobilization and supergene enrichment during groundwater-regolith interaction:
Geochimica et Cosmochimica Acta.

et al., 2019), are all predicted to dissolve spontaneously in the mildly acidic regolith water (Table 1). Gadolinite-(Y) and hingganite-(Y), however, are predicted to be insoluble in the alkaline aquifer groundwater, emphasizing the control exercised by pH on REE mineral dissolution. In contrast, xenotime-(Y), fergusonite-(Y), and zircon are predicted to be insoluble even in the regolith water, consistent with the observation that they are the most common detrital minerals in the regolith at Zudong (Li et al., 2019).

At Bankeng, fluor-apatite, monazite-(Ce), and LREE-fluorocarbonates are the main hosts to the REE in the parent granite and, as apatite and LREE-fluorocarbonates are not present in the regolith, these minerals have been interpreted to be the source of the LREE for the latter (Li et al., 2020). The thermodynamic data for bastnäsite-(Ce) yield contradictory predictions. A comparison of log Q to log K for bastnäsite-(Ce), based on the thermodynamic data of Ai-Nafai et al. (2019), predicts that bastnäsite-(Ce) should dissolve in the regolith water, consistent with its absence from the regolith, whereas the log K value obtained using the data of Gysi and Williams-Jones (2015) predicts the opposite (Table 2). A comparison for parisite-(Ce), based on thermodynamic data from Gysi and Williams-Jones (2015), predicts that this REE mineral is also insoluble. It is noteworthy, however, that the comparison for synchysite-(Ce), based on the thermodynamic data obtained in the present study, predicts that this LREE fluorocarbonate mineral should dissolve (Table 2). Although, the same comparison cannot be made for REE-bearing fluorapatite, comparison of log Q with log K for fluor-apatite predicts that this mineral should be insoluble in the regolith water (Table 1); monazite-(Ce) is also predicted to be insoluble, which is to be expected as it is a common detrital mineral in the regolith. The present study is therefore unable to reliably predict the source REE in the Bankeng regolith, beyond observing that there is some evidence that the LREE fluoro-carbonates may be thermodynamically unstable in the regolith water. The absence of fluor-apatite in the regolith does require explanation and a possibility is that it contained sufficient Th and or U to make it

Li, M. Y. H., Kwong, H. T., Williams-Jones, A. E., and Zhou, M.-F., 2021,
The thermodynamics of rare earth element liberation, mobilization and supergene enrichment during groundwater-regolith interaction:
Geochimica et Cosmochimica Acta.

metamict (Pan and Fleet, 2002) and, thus, sufficiently unstable to dissolve in the regolith water. It is also possible that this explanation may apply to the LREE fluorocarbonates, which in some cases have been shown to contain several weight % REE (Förster, 2001; Beland and Williams-Jones, 2020).

Some common LREE minerals that are predicted to be thermodynamically unstable during weathering, based on their positive log Ksp values, are allanite-(Ce), titanite, eudialyte, chevkinite-(Ce), and loparite-(Ce) (Table 1). Though these minerals are not observed in the protolith of either the Zudong or Bankeng deposits, it is noteworthy, based on a comparison of the log K values for their dissolution reactions and the logQ values calculated from the regolith waters of Zudong and Bankeng that these minerals are predicted to dissolve and thus are likely to be potential sources for regolith-hosted ion-adsorption deposits elsewhere.

5.1.3 REE enrichment in regolith

After liberation of the REE from the protolith minerals to surface waters, interaction of these waters with the regolith may enrich the latter in REE through adsorption and mineral precipitation, with adsorption exercising the main control on REE ore formation. In the Zudong deposit, the clay-sorbed fraction is characterized by negative Y anomalies (0.70 – 0.84; Fig. 4a and Table S5). However, these anomalies are absent in the bulk regolith samples (0.93 – 1.05; Table S5) and the bulk regolith water (1.24; Table S5). Moreover, the positive Y anomaly of 1.19 in the parent granite indicates that the negative anomaly in the clay-sorbed fraction is not an inherited feature. This, implies that the anomalously low concentration of Y in the clay-sorbed fraction is due to the stability of the corresponding surface complex being lower than that of Ho and Er. Support for this interpretation is provided by the observation that the concentration of the Y^{3+} fraction of the bulk Y in the regolith water is anomalously high, suggesting that Y was not as efficiently removed from this water as Ho and Er (Fig. 5b). An

Li, M. Y. H., Kwong, H. T., Williams-Jones, A. E., and Zhou, M.-F., 2021,
The thermodynamics of rare earth element liberation, mobilization and supergene enrichment during groundwater-regolith interaction: Geochimica et Cosmochimica Acta.

435 analogous interpretation can be made for Sm, which is characterized by a positive anomaly in
436 the clay-sorbed fraction (1.38 – 1.58; Table S6) and a negative anomaly for the Sm^{3+} fraction
437 of the regolith water (Fig. 5b). Similar conclusions can be drawn from the Bankeng deposit in
438 which: 1) the clay-sorbed REE fraction is characterized by positive anomalies for Gd, Y, and
439 Yb (Fig. 4b); 2) these anomalies are absent in the bulk regolith and the parent granite (Table
440 S6) and; 3) the concentration of the $REE(CO_3)_2^-$ fraction of the bulk Gd, Y, and Yb in the
441 regolith water is anomalously low, suggesting that these elements were more efficiently
442 removed from this water that adjacent elements in the REE profile (Fig. 6a)..
443
444 ***5.1.4 A Plausible REE sorption scenario***
445 Accumulation of HREEs in regolith is generally not favored (e.g., Braun et al., 1998;
446 Nesbitt, 1979; Yusoff et al., 2013). In regolith-hosted HREE deposits, however, the HREEs
447 are retained in sufficient concentrations to form economic deposits (Li et al., 2017).
448 Considering the ease with which the REEs are extracted from these deposits, outer-sphere
449 complexation should be important for the REE sorption (Li et al., 2017). In this study, we have
450 demonstrated that anomalous enrichment of some of the REEs in the clay-sorbed fractions may
451 be related to the relative stability of particular REE species in the regolith water (REE^{3+} at
452 Zudong and $REE(CO_3)_2^-$ at Bankeng). In Li and Zhou (2020), a positive causal relationship
453 between the clay-adsorbed HREE concentration and the proportion of halloysite in the
454 regolithg. We therefore propose, in the case of the Zudong deposit that the REE were adsorbed
455 primarily as surface complexes involving REE^{3+} on the halloysite surface, whereas at Bankeng
456 they were adsorbed as $REE(CO_3)_2^-$ at interlayer sites in the halloysite. Support for the former
457 hypothesis is provided by two studies showing that hydrated REE^{3+} are adsorbed as outer-
458 sphere complexes at the edges and in basal sites of halloysite and kaolinite (Borst et al., 2020;
459 Yamaguchi et al., 2018) and the latter hypothesis seems plausible given that halloysite is a

Li, M. Y. H., Kwong, H. T., Williams-Jones, A. E., and Zhou, M.-F., 2021,
The thermodynamics of rare earth element liberation, mobilization and supergene enrichment during groundwater-regolith interaction:
Geochimica et Cosmochimica Acta.

460 hydrated mineral with a layer of easily exchangeable water molecules between TO silicate
461 sheets.

462 Incorporation of salts as interlayer complexes in halloysite has been shown to be
463 feasible only for larger cations and anions (Wada, 1959b). The CO_3^{2-} ion (ionic radius = 1.78
464 Å; Jenkins and Thakur, 1979) is larger than the Cl^- ion (ionic radius = 1.67 Å, VI co-ordination;
465 Shannon, 1976), which has been shown to occupy interlayer sites in halloysite (Wada, 1959a),
466 although the ionic radii of the REE^{3+} ions (between 1 and 1.2 Å, VI co-ordination; Shannon,
467 1976) are smaller than the ionic radius of K^+ (1.52 Å, VI co-ordination; Shannon, 1976), a
468 cation that has been shown to occupy these interlayer sites. The $REE(CO_3)_2^-$ ion, however,
469 would be much larger (ionic radius < 4 Å, the sum of the radii of the contributing ions) but
470 less than half the width of the interlayers (10.9 Å; Hillier and Ryan, 2002). Incorporation of
471 $REE(CO_3)_2^-$ therefore appears feasible. We also suspect that additional stability would be
472 gained by adsorption of the HREE cations in the hexagonal cavity at the basal surface of the
473 tetrahedral sheet of halloysite, with the carbonate ions orienting themselves around the
474 adsorbed cations. In summary, the evidence presented above and the preceding section (5.1.3)
475 makes a compelling case that the REE were adsorbed as simple ions by surface complexation
476 on halloysite at Zudong and as $REE(CO_3)_2^-$ that replaced interlayer water at Bankeng.
477

478 **5.2 Factors controlling REE mobility during weathering**

479 ***5.2.1 Lithological factors***

480 The nature of the protolith, as the source of the REE entering the supergene
481 environment, is a first order determinant for the formation of an economic REE deposit.
482 Whether an economic deposit will form depends both on the absolute concentration of the REE
483 in the protolith as well as the extent to which they can be mobilized. In most cases, the REEs
484 are hosted by accessory minerals and, therefore, the stability of these minerals will determine

Li, M. Y. H., Kwong, H. T., Williams-Jones, A. E., and Zhou, M.-F., 2021,
The thermodynamics of rare earth element liberation, mobilization and supergene enrichment during groundwater-regolith interaction:
Geochimica et Cosmochimica Acta.

485 if large-scale REE liberation is possible. Enrichment of the REE is commonly observed where
486 the regolith results from the weathering of felsic igneous rocks, including granite, syenite,
487 rhyolite, and tuff (e.g., Berger et al., 2014; Fu et al., 2019; Li et al., 2019, 2020; Sanematsu et
488 al., 2013). In these protoliths, allanite-(Ce), titanite, and apatite commonly occur as accessory
489 minerals, and high abundance of these minerals indicates a fertile protolith for ore formation.
490 Agpaitic peralkaline and alkaline rocks are particularly good sources of easily liberated REE
491 because refractory REE-bearing minerals like zircon are replaced by minerals like the alkali-
492 zirconoslicates across the miaskitic to agpaitic transition that are much more susceptible to
493 alteration (Vasyukova and Williams-Jones, 2020). As discussed earlier, eudialyte is unstable
494 during weathering (Table 1) and is able to release its REEs for enrichment in the regolith.
495 Although carbonatites are characterized by high REE concentrations and host some of the
496 World's largest economic REE deposits, they are not good sources for regolith-hosted REE
497 deposits. This is because, based on our calculations, their main REE minerals, bastnäsite-(Ce),
498 parisite-(Ce), monazite, and apatite (Verplanck et al., 2016), are resistant to dissolution by
499 weathering fluids. An example of this is provided by the Dalucao carbonatite deposit in SW
500 China, where the above mentioned REE minerals have been concentrated to exploitable levels
501 in the regolith only because of the dissolution of calcite during weathering (Liu et al., 2015).

502 Hydrothermal alteration of the protolith prior to weathering could make it a more
503 favorable source for the REE, by elevating the bulk REE concentration and/or converting the
504 REE mineral assemblage to one that is more susceptible to weathering (Li et al., 2017;
505 Sanematsu and Watanabe, 2016). This was the case for the Zudong deposit, where the main
506 HREE minerals in the parent granite, synchysite-(Y), gadolinite-(Y), and hingganite-(Y), are
507 hydrothermal in origin (Li et al., 2019) and are unstable during weathering. In other cases,
508 however, hydrothermal alteration may have the opposite effect. For example, in the Casto
509 granite, Idaho, USA, primary allanite-(Ce), a mineral that is predicted to be susceptible to

Li, M. Y. H., Kwong, H. T., Williams-Jones, A. E., and Zhou, M.-F., 2021,
The thermodynamics of rare earth element liberation, mobilization and supergene enrichment during groundwater-regolith interaction:
Geochimica et Cosmochimica Acta.

weathering (Table 1) was replaced hydrothermally by monazite-(Ce), which as discussed previously, is resistant to weathering (Wood and Ricketts, 2000). During regional metamorphism, the coupled dissolution of monazite-(Ce) and precipitation of fluor-apatite and allanite-(Ce) in the presence of Ca-rich fluids is a common phenomenon up to amphibolite facies (Budzyń et al., 2011), but at higher metamorphic grade, monazite-(Ce) is more stable than allanite-(Ce) and apatite (Janots et al., 2008). Hence, tracing the reaction pathways of metasomatism and metamorphism is crucial to evaluating the protolith fertility for REE liberation and supergene ore formation.

5.2.2 Hydrogeological factor

Supergene REE mobility and fractionation are controlled mainly by the aqueous REE speciation which, in turn, is controlled by ligand availability and pH. In acidic groundwater, REEs occur mainly as simple hydrated cations, except if the SO_4^{2-} and F^- concentrations are high, in which case $REESO_4^+$ and $REEF^{2+}$ may also be important in controlling REE mobility (Wood, 1990). It is important to note, however, that REE adsorption by clay minerals is inhibited because of competition from H^+ (Coppin et al., 2002). In circum-neutral and alkaline groundwaters, REE-carbonate species become much more important (Johannesson et al., 1996; Wood, 1990). Also, REE adsorption on clay minerals is favored because of the low concentration of H^+ ions (Coppin et al., 2002; Yang et al., 2019). Although adsorption experiments have not detected discernible REE fractionation during adsorption of REE^{3+} on kaolinite or halloysite at low ionic strength (Coppin et al., 2002; Yang et al., 2019), field studies, particularly of near neutral and alkaline groundwater, in which REE-carbonate species are important in controlling REE mobility, have shown that fractionation of the REE is appreciable (Johannesson et al., 1996; Johannesson et al., 2000). The LREEs are preferentially removed from groundwater through adsorption on clay minerals, whereas the HREEs remain in solution

Li, M. Y. H., Kwong, H. T., Williams-Jones, A. E., and Zhou, M.-F., 2021,
The thermodynamics of rare earth element liberation, mobilization and supergene enrichment during groundwater-regolith interaction:
Geochimica et Cosmochimica Acta.

because of strong HREE-carbonate complexation (Johannesson et al., 2000; Tang and Johannesson, 2010). Thus, pH and carbonate concentration are important controls on REE deportment in the regolith. In the Zudong deposit, the regolith water is slightly acidic and has a relatively low carbonate content (31 mg/L HCO_3^-), whereas at Bankeng, the regolith water is circum-neutral and the carbonate content is nearly five times higher (146 mg/L HCO_3^-) than at Zudong (Table 3). The deep aquifer water, in contrast, is slightly alkaline and has a carbonate content of 573 mg/L HCO_3^- (Table 3). It is therefore likely that this was the main carbonate source for the shallow regolith waters at both deposits. At Zudong, where the carbonate content in the regolith water is low, presumably because of less mixing with the aquifer water, the REE were transported dominantly as simple hydrated ions (Fig. 5). Consequently, the HREE were not preferentially removed, thereby permitting their concentration in the regolith. At Bankeng, however, where the carbonate content was much higher, due probably to greater mixing of the regolith water with the aquifer water, the REE were transported dominantly as carbonate complexes (Fig. 6), thereby increasing the proportion of LREE available for adsorption by the clay minerals. In summary, pH and the carbonate concentration of the regolith water affect REE adsorption and the fractionation of the LREE from the HREE fractionation, either because of the aqueous REE speciation and/or the adsorption mechanism and, in the case of Zudong and Bankeng, this was significantly affected by the degree of mixing of the regolith and aquifer waters.

5.3 The use of REEs in probing chemical weathering processes

The regolith is commonly enriched in LREEs, whereas the HREEs are largely lost to groundwater and rivers (e.g., Aubert et al., 2001; Braun et al., 1993; Braun et al., 1998; Johannesson et al., 1996; Nesbitt, 1979). In some cases, there is a weak enrichment of HREEs in the regolith but this is mainly due to the accumulation of residual zircon and xenotime (e.g.,

Li, M. Y. H., Kwong, H. T., Williams-Jones, A. E., and Zhou, M.-F., 2021,
The thermodynamics of rare earth element liberation, mobilization and supergene enrichment during groundwater-regolith interaction: Geochimica et Cosmochimica Acta.

Murakami and Ishihara, 2008). Thus, LREE-HREE fractionation increases with progressive weathering (Ma et al., 2007; Nesbitt, 1979; Yusoff et al., 2013), except for the topsoil, which is often subjected to intense leaching and near complete removal of all REEs. If, however, the clay mineralogy is suitable, for example halloysite in the Zudong deposit, the HREEs can be efficiently adsorbed and retained in the regolith (Li and Zhou, 2020). Our study shows that the interplay between aqueous complexation in groundwater and adsorption on clay minerals in the regolith controls the enrichment and/or depletion of the REE, as well as their fractionation. It is, thus, necessary to consider these factors when evaluating the REE distribution in soil profiles during the exploration for regolith-hosted REE deposits.

A progressive depletion of Y relative to Ho is widely observed in basaltic soil profiles, suggesting that it may be possible to use the Y/Ho ratio as a proxy for silicate weathering (Babechuk et al., 2015). This phenomenon has been attributed to the anomalously low affinity of Y for Fe oxides and therefore, the preferential loss of Y during progressive weathering (Babechuk et al., 2015; Thompson et al., 2013). At Bankeng, however, the opposite is observed, i.e., there is a trend of increasing Y/Ho ratio in the regolith above the lower saprolite. As the abundance of Fe oxides in regoliths above granitic rocks is expected to be lower than above mafic rocks, the effect of Fe oxides on Y/Ho fractionation is probably weaker. This, however, does not explain the negative Y anomaly in the Zudong regolith. Instead, it seems more likely that whether a negative or positive Y/Ho anomaly develops in the regolith over granitic rocks depends mainly on the pH and carbonate content of the regolith water as discussed earlier.

6. Conclusions

Positive values of the logarithm of the solubility product of some important REE-bearing minerals, namely synchysite-(Y), gadolinite-(Y), hingganite-(Y), yttrialite-(Y), allanite-(Ce), titanite, eudialyte, chevkinite-(Ce), and loparite-(Ce) predict that they will

Li, M. Y. H., Kwong, H. T., Williams-Jones, A. E., and Zhou, M.-F., 2021,
The thermodynamics of rare earth element liberation, mobilization and supergene enrichment during groundwater-regolith interaction:
Geochimica et Cosmochimica Acta.

585 dissolve spontaneously in water. Hence, rocks with high abundances of these minerals could
586 release large concentrations of REEs to solution during weathering. Such rocks are, therefore,
587 fertile sources for regolith-hosted HREE or LREE deposits. Weathering of apatite, monazite,
588 and synchysite-(Ce) may depend on the mineral crystallinity. Common REE minerals like
589 monazite-(Ce) and LREE-fluorocarbonates, such as bastnäsite-(Ce) and parisite-(Ce), are
590 predicted to resist dissolution, and therefore could form residual REE deposits but not regolith-
591 hosted ion adsorption deposits. We have shown that the regolith water is slightly acidic in the
592 Zudong deposit and circum-neutral and carbonate-rich in the Bankeng deposit. The pH and
593 carbonate concentration exercised a major control on the REE mobility and adsorption by clay
594 minerals at these two sites, with the simple ion and surface complexation dominating at Zudong
595 (lower pH and carbonate concentration) and carbonate species and their interlayer clay mineral
596 incorporation dominating at Bankeng (higher pH and carbonate concentration). These two
597 factors are in turn, being influenced by the degree of mixing of the regolith water with local
598 deep-circulating alkaline and carbonate-rich groundwater at the two sites (low at Zudong and
599 high at Bankeng). The combination of an appropriate protolith mineralogy and favorable
600 hydrogeological conditions are thus essential for the efficient adsorption of the HREE on clay
601 minerals in the regolith to form the economic deposits that now provide the global endowment
602 of HREEs. Finally, as the interplay of aqueous complexation with the regolith mineralogy
603 significantly affects LREE-HREE and Y-Ho fractionation during groundwater-regolith
604 interaction, a comprehensive understanding of this behavior of the REEs is needed before using
605 them to probe chemical weathering processes.
606

607 **Acknowledgements**

608 Mr Wenzhao Liang provided help with the water analysis and Dr. Hoi Chim Chiu and
609 Mr Johnson Yeung provided access to the TOC analyzer at HKBU. This study was supported

Li, M. Y. H., Kwong, H. T., Williams-Jones, A. E., and Zhou, M.-F., 2021,
The thermodynamics of rare earth element liberation, mobilization and supergene enrichment during groundwater-regolith interaction:
Geochimica et Cosmochimica Acta.

financially by a grant from a Major Research Plan of the Natural Science Foundation of China (91962216) to M.-F.Z and a Visiting Professorship of HKU to A.W-J.

References

Al-Nafai, I., Kim, H. and Osseo-Asare, K. (2019) Estimation of the standard free energy of formation of bastnasite, REFCO 3. Mining, Metallurgy & Exploration 36, 227-233.

Aubert, D., Stille, P. and Probst, A. (2001) REE fractionation during granite weathering and removal by waters and suspended loads: Sr and Nd isotopic evidence. Geochimica et Cosmochimica Acta 65, 387-406.

Babechuk, M., Widdowson, M., Murphy, M. and Kamber, B. (2015) A combined Y/Ho, high field strength element (HFSE) and Nd isotope perspective on basalt weathering, Deccan Traps, India. Chemical Geology 396, 25-41.

Berger, A., Janots, E., Gnos, E., Frei, R. and Bernier, F. (2014) Rare earth element mineralogy and geochemistry in a laterite profile from Madagascar. Applied Geochemistry 41, 218-228.

Borst, A.M., Smith, M.P., Finch, A.A., Estrade, G., Villanova-de-Benavent, C., Nason, P., Marquis, E., Horsburgh, N.J., Goodenough, K.M. and Xu, C. (2020) Adsorption of rare earth elements in regolith-hosted clay deposits. Nature communications 11, 1-15.

Braun, J.-J., Pagel, M., Herbilln, A. and Rosin, C. (1993) Mobilization and redistribution of REEs and thorium in a syenitic lateritic profile: a mass balance study. Geochimica et Cosmochimica Acta 57, 4419-4434.

Braun, J.-J., Viers, J., Dupré, B., Polve, M., Ndam, J. and Muller, J.-P. (1998) Solid/liquid REE fractionation in the lateritic system of Goyoum, East Cameroon: the implication for the present dynamics of the soil covers of the humid tropical regions. Geochimica et Cosmochimica Acta 62, 273-299.

Li, M. Y. H., Kwong, H. T., Williams-Jones, A. E., and Zhou, M.-F., 2021,
The thermodynamics of rare earth element liberation, mobilization and supergene enrichment during groundwater-regolith interaction: Geochimica et Cosmochimica Acta.

635 Budzyń, B., Harlov, D.E., Williams, M.L. and Jercinovic, M.J. (2011) Experimental
636 determination of stability relations between monazite, fluorapatite, allanite, and REE-epidote
637 as a function of pressure, temperature, and fluid composition. American Mineralogist 96,
638 1547-1567.
639 Chermak, J.A. and Rimstidt, J.D. (1989) Estimating the thermodynamic properties (ΔG^{0f} and
640 ΔH^{0f}) of silicate minerals at 298 K from the sum of polyhedral contributions. American
641 Mineralogist 74, 1023-1031.
642 Coppin, F., Berger, G., Bauer, A., Castet, S. and Loubet, M. (2002) Sorption of lanthanides
643 on smectite and kaolinite. Chemical Geology 182, 57-68.
644 da Silva, Y.J.A.B., do Nascimento, C.W.A., Biondi, C.M., van Straaten, P., de Souza Júnior,
645 V.S., da Silva, Y.J.A.B., dos Santos, C.A. and de Araújo, J.d.C.T. (2017) Influence of
646 metaluminous granite mineralogy on the rare earth element geochemistry of rocks and soils
647 along a climosequence in Brazil. Geoderma 306, 28-39.
648 Elderfield, H., Upstill-Goddard, R. and Sholkovitz, E. (1990) The rare earth elements in
649 rivers, estuaries, and coastal seas and their significance to the composition of ocean waters.
650 Geochimica et Cosmochimica Acta 54, 971-991.
651 Emsbo, P., McLaughlin, P.I., du Bray, E.A., Anderson, E.D., Vandenbroucke, T. and
652 Zielinski, R.A. (2016) Rare earth elements in sedimentary phosphorite deposits: a global
653 assessment. Reviews in Economic Geology 18, 101-113.
654 Förster, H.-J. (2001) Synchysite-(Y)–synchysite-(Ce) solid solutions from Markersbach,
655 Erzgebirge, Germany: REE and Th mobility during high-T alteration of highly fractionated
656 aluminous A-type granites. Mineralogy and Petrology 72, 259-280.
657 Fu, W., Luo, P., Hu, Z., Feng, Y., Liu, L., Yang, J., Feng, M., Yu, H. and Zhou, Y. (2019)
658 Enrichment of ion-exchangeable rare earth elements by felsic volcanic rock weathering in

Li, M. Y. H., Kwong, H. T., Williams-Jones, A. E., and Zhou, M.-F., 2021,
The thermodynamics of rare earth element liberation, mobilization and supergene enrichment during groundwater-regolith interaction:
Geochimica et Cosmochimica Acta.

659 South China: Genetic mechanism and formation preference. Ore Geology Reviews 114,
660 103120.
661 Gysi, A.P. and Williams-Jones, A.E. (2015) The thermodynamic properties of bastnäsite-(Ce)
662 and parisite-(Ce). Chemical Geology 392, 87-101.
663 Haas, J.R., Shock, E.L. and Sassani, D.C. (1995) Rare earth elements in hydrothermal
664 systems: estimates of standard partial molal thermodynamic properties of aqueous complexes
665 of the rare earth elements at high pressures and temperatures. Geochimica et Cosmochimica
666 Acta 59, 4329-4350.
667 HACH. (2018) Alkalinity, Phenolphthalein and Total Alkalinity Method 8203, Digital
668 Titrator. Hach Company, p. 8.
669 Hazen, R.M. (1988) A useful fiction: polyhedral modeling of mineral properties. American
670 Journal of Science 288, 242-269.
671 Hoskin, P.W., Kinny, P.D., Wyborn, D. and Chappell, B.W. (2000) Identifying accessory
672 mineral saturation during differentiation in granitoid magmas: an integrated approach.
673 Journal of Petrology 41, 1365-1396.
674 Janots, E., Engi, M., Berger, A., Allaz, J., Schwarz, J.O. and Spandler, C. (2008) Prograde
675 metamorphic sequence of REE minerals in pelitic rocks of the Central Alps: implications for
676 allanite–monazite–xenotime phase relations from 250 to 610 C. Journal of Metamorphic
677 Geology 26, 509-526.
678 Jenkins, H.D.B. and Thakur, K.P. (1979) Reappraisal of thermochemical radii for complex
679 ions. Journal of Chemical Education 56, 576-577.
680 Johannesson, K.H., Farnham, I.M., Guo, C. and Stetzenbach, K.J. (1999) Rare earth element
681 fractionation and concentration variations along a groundwater flow path within a shallow,
682 basin-fill aquifer, southern Nevada, USA. Geochimica et Cosmochimica Acta 63, 2697-2708.

683 Johannesson, K.H., Stetzenbach, K.J., Hodge, V.F. and Lyons, W.B. (1996) Rare earth
684 element complexation behavior in circumneutral pH groundwaters: assessing the role of
685 carbonate and phosphate ions. Earth and Planetary Science Letters 139, 305-319.
686 Johannesson, K.H., Zhou, X., Guo, C., Stetzenbach, K.J. and Hodge, V.F. (2000) Origin of
687 rare earth element signatures in groundwaters of circumneutral pH from southern Nevada and
688 eastern California, USA. Chemical Geology 164, 239-257.
689 Kondrat'eva, O.N., Nikiforova, G.E., Tyurin, A.V., Khoroshilov, A.V., Gurevich, V.M. and
690 Gavrichev, K.S. (2019) Thermodynamic properties of, and fergusonite-to-scheelite phase
691 transition in, gadolinium orthoniobate GdNbO4 ceramics. Journal of Alloys and Compounds
692 779, 660-666.
693 Laveuf, C. and Cornu, S. (2009) A review on the potentiality of rare earth elements to trace
694 pedogenetic processes. Geoderma 154, 1-12.
695 Li, M.Y.H. and Zhou, M.-F. (2020) The role of clay minerals in formation of the regolith-
696 hosted heavy rare earth element deposits. American Mineralogist 105, 92-108.
697 Li, M.Y.H., Zhou, M.-F. and Williams-Jones, A.E. (2019) The genesis of regolith-hosted
698 heavy rare earth element deposits: Insights from the world-class Zudong deposit in Jiangxi
699 Province, South China. Economic Geology 114, 541-568.
700 Li, M.Y.H., Zhou, M.-F. and Williams-Jones, A.E. (2020) Controls on the dynamics of rare
701 earth elements during sub-tropical hillslope processes and formation of regolith-hosted
702 deposits. Economic Geology 115, 1097-1118.
703 Li, X.-C. and Zhou, M.-F. (2017) Hydrothermal alteration of monazite-(Ce) and chevkinite-
704 (Ce) from the Sin Quyen Fe-Cu-LREE-Au deposit, northwestern Vietnam. American
705 Mineralogist: Journal of Earth and Planetary Materials 102, 1525-1541.

Li, M. Y. H., Kwong, H. T., Williams-Jones, A. E., and Zhou, M.-F., 2021,
The thermodynamics of rare earth element liberation, mobilization and supergene enrichment during groundwater-regolith interaction:
Geochimica et Cosmochimica Acta.

706 Li, Y.H.M., Zhao, W.W. and Zhou, M.-F. (2017) Nature of parent rocks, mineralization
707 styles and ore genesis of regolith-hosted REE deposits in South China: An integrated genetic
708 model. Journal of Asian Earth Sciences 148, 65-95.
709 Liu, Y., Zhu, Z., Chen, C., Zhang, S., Sun, X., Yang, Z. and Liang, W. (2015) Geochemical
710 and mineralogical characteristics of weathered ore in the Dalucao REE deposit, Mianning–
711 Dechang REE Belt, western Sichuan Province, southwestern China. Ore Geology Reviews
712 71, 437-456.
713 Lottermoser, B. (1990) Rare-earth element mineralisation within the Mt. Weld carbonatite
714 laterite, Western Australia. Lithos 24, 151-167.
715 Luo, Y.-R. and Byrne, R.H. (2004) Carbonate complexation of yttrium and the rare earth
716 elements in natural waters. Geochimica et Cosmochimica Acta 68, 691-699.
717 Ma, J.-L., Wei, G.-J., Xu, Y.-G., Long, W.-G. and Sun, W.-D. (2007) Mobilization and re-
718 distribution of major and trace elements during extreme weathering of basalt in Hainan
719 Island, South China. Geochimica et Cosmochimica Acta 71, 3223-3237.
720 Meldrum, A., Boatner, L., Weber, W. and Ewing, R. (1998) Radiation damage in zircon and
721 monazite. Geochimica et Cosmochimica Acta 62, 2509-2520.
722 Möller, V. and Williams-Jones, A.E. (2017) Magmatic and hydrothermal controls on the
723 mineralogy of the basal zone, Nechalacho REE-Nb-Zr deposit, Canada. Economic Geology
724 112, 1823-1856.
725 Murakami, H. and Ishihara, S. (2008) REE mineralization of weathered crust and clay
726 sediment on granitic rocks in the Sanyo Belt, SW Japan and the Southern Jiangxi Province,
727 China. Resource Geology 58, 373-401.
728 Nesbitt, H.W. (1979) Mobility and fractionation of rare earth elements during weathering of a
729 granodiorite. Nature 279, 206-210.

Li, M. Y. H., Kwong, H. T., Williams-Jones, A. E., and Zhou, M.-F., 2021,
The thermodynamics of rare earth element liberation, mobilization and supergene enrichment during groundwater-regolith interaction:
Geochimica et Cosmochimica Acta.

730 Nikiforova, G., Khoroshilov, A., Tyurin, A., Gurevich, V. and Gavrichev, K. (2019) Heat
731 capacity and thermodynamic properties of lanthanum orthoniobate. The Journal of Chemical
732 Thermodynamics 132, 44-53.
733 Pan, Y. and Fleet, M.E. (2002) Compositions of the apatite-group minerals: substitution
734 mechanisms and controlling factors. Reviews in Mineralogy and Geochemistry 48, 13-49.
735 Parkhurst, D.L. and Appelo, C. (2013) Description of input and examples for PHREEQC
736 version 3: a computer program for speciation, batch-reaction, one-dimensional transport, and
737 inverse geochemical calculations. US Geological Survey, p. 497.
738 Reznitskii, L.A. (2001) Formation enthalpies of Nb (IV, V) oxide compounds. Inorganic
739 Materials 37, 491-495.
740 Sanematsu, K., Kon, Y., Imai, A., Watanabe, K. and Watanabe, Y. (2013) Geochemical and
741 mineralogical characteristics of ion-adsorption type REE mineralization in Phuket, Thailand.
742 Mineralium Deposita 48, 437-451.
743 Sanematsu, K. and Watanabe, Y. (2016) Characteristics and genesis of ion-adsorption type
744 deposits. Reviews in Economic Geology 18, 55-79.
745 Shannon, R.D. (1976) Revised effective ionic radii and systematic studies of interatomic
746 distances in halides and chalcogenides. Acta Crystallographica Section A: Crystal physics,
747 diffraction, theoretical and general crystallography 32, 751-767.
748 Sheard, E.R., Williams-Jones, A.E., Heiligmann, M., Pederson, C. and Trueman, D.L. (2012)
749 Controls on the concentration of zirconium, niobium, and the rare earth elements in the Thor
750 Lake rare metal deposit, Northwest Territories, Canada. Economic Geology 107, 81-104.
751 Shvarov, Y.V. (1999) Algorithmization of the numeric equilibrium modeling of dynamic
752 geochemical processes. Geochemistry International 37, 571-576.

Li, M. Y. H., Kwong, H. T., Williams-Jones, A. E., and Zhou, M.-F., 2021,
The thermodynamics of rare earth element liberation, mobilization and supergene enrichment during groundwater-regolith interaction:
Geochimica et Cosmochimica Acta.

753 Smith, M., Moore, K., Kavecsánszki, D., Finch, A.A., Kynicky, J. and Wall, F. (2016) From
754 mantle to critical zone: A review of large and giant sized deposits of the rare earth elements.
755 Geoscience Frontiers 7, 315-334.
756 Tang, J. and Johannesson, K.H. (2010) Rare earth elements adsorption onto Carrizo sand:
757 Influence of strong solution complexation. Chemical Geology 279, 120-133.
758 Thompson, A., Amistadi, M.K., Chadwick, O.A. and Chorover, J. (2013) Fractionation of
759 yttrium and holmium during basaltic soil weathering. Geochimica et Cosmochimica Acta
760 119, 18-30.
761 Vasyukova, O. and Williams-Jones, A. (2020) Partial melting, fractional crystallisation,
762 liquid immiscibility and hydrothermal mobilisation–A 'recipe'for the formation of economic
763 A-type granite-hosted HFSE deposits. Lithos 356, 105300.
764 Verplanck, P., Mariano, A. and Mariano Jr, A. (2016) Rare earth element ore geology of
765 carbonatites. Rev. Econ. Geol 18, 5-32.
766 Verplanck, P.L. and Van Gosen, B.S. (2011) Carbonatite and alkaline intrusion-related rare
767 earth element deposits–a deposit model. US Geological Survey.
768 Voigt, M., Rodriguez-Blanco, J.D., Vallina, B., Benning, L.G. and Oelkers, E.H. (2016) An
769 experimental study of hydroxylbastnasite solubility in aqueous solutions at 25 C. Chemical
770 Geology 430, 70-77.
771 Wada, K. (1959a) An interlayer complex of halloysite with ammonium chloride. American
772 Mineralogist: Journal of Earth and Planetary Materials 44, 1237-1247.
773 Wada, K. (1959b) Oriented penetration of ionic compounds between the silicate layers of
774 halloysite. American Mineralogist: Journal of Earth and Planetary Materials 44, 153-165.
775 Williams-Jones, A. and Migdisov, A. (2014) Experimental constraints on the transport and
776 deposition of metals in ore-forming hydrothermal systems. Society of Economic Geologists
777 Special Publication 18, 77-95.

Li, M. Y. H., Kwong, H. T., Williams-Jones, A. E., and Zhou, M.-F., 2021,
The thermodynamics of rare earth element liberation, mobilization and supergene enrichment during groundwater-regolith interaction:
Geochimica et Cosmochimica Acta.

778 Williams-Jones, A.E., Migdisov, A.A. and Samson, I.M. (2012) Hydrothermal mobilisation
779 of the rare earth elements–a tale of "ceria" and "yttria". Elements 8, 355-360.
780 Wood, S.A. (1990) The aqueous geochemistry of the rare-earth elements and yttrium: 1.
781 Review of available low-temperature data for inorganic complexes and the inorganic REE
782 speciation of natural waters. Chemical Geology 82, 159-186.
783 Wood, S.A. and Ricketts, A. (2000) Allanite-(Ce) from the Eocene Casto granite, Idaho:
784 response to hydrothermal alteration. The Canadian Mineralogist 38, 81-100.
785 Wu, C. (1988) The study of ion-adsorbed type of rare earth deposits in weathering crust from
786 south Jiangxi and north Guangdong provinces, Graduate School, Chinese Academy of
787 Geological Sciences. Graduate School, Chinese Academy of Geological Sciences, Beijing, p.
788 158 (in Chinese with English abstract).
789 Yamaguchi, A., Honda, T., Tanaka, M., Tanaka, K. and Takahashi, Y. (2018) Discovery of
790 ion-adsorption type deposits of rare earth elements (REE) in Southwest Japan with speciation
791 of REE by extended X-ray absorption fine structure spectroscopy. Geochemical Journal 52,
792 415-425.
793 Yang, M., Liang, X., Ma, L., Huang, J., He, H. and Zhu, J. (2019) Adsorption of REEs on
794 kaolinite and halloysite: A link to the REE distribution on clays in the weathering crust of
795 granite. Chemical Geology 525, 210-217.
796 Yusoff, Z.M., Ngwenya, B.T. and Parsons, I. (2013) Mobility and fractionation of REEs
797 during deep weathering of geochemically contrasting granites in a tropical setting, Malaysia.
798 Chemical Geology 349, 71-86.

799

Li, M. Y. H., Kwong, H. T., Williams-Jones, A. E., and Zhou, M.-F., 2021,
The thermodynamics of rare earth element liberation, mobilization and supergene enrichment during groundwater-regolith interaction:
Geochimica et Cosmochimica Acta.

800 **Figure captions**

801 **Figure 1**. Simplified geological map of the Zudong and Bankeng deposits (after Li et al., 2019).
802 The high-grade ore zone of the Zudong deposit and the exploration area for a potential high-
803 grade zone in the Bankeng deposit are also indicated.

804

805 **Figure 2**. (a) - (d) Backscattered (BSE) images showing the occurrence of common HREE
806 minerals in the parent granite of the Zudong deposit. (a) Synchysite-(Y) and fluorite replacing
807 albite and K-feldspar. (b) Gadolinite-(Y) and yttrialite-(Y) replacing albite. (c) Hingganite-(Y)
808 replacing albite along cleavages. (d) An intergrowth of fergusonite-(Y) and xenotime.
809 Abbreviations: Ab: albite; Fgt: fergusonite-(Y), Fl: fluorite, Gad: gadolinite-(Y), Hgt:
810 hingganite-(Y), Kfs: K-feldspar, Sct: synchysite-(Y), Xnm: xenotime, Ytt: yttrialite-(Y).

811

812 **Figure 3**. (a) - (d) Backscattered (BSE) images showing the occurrence of common LREE
813 minerals in the parent granite of the Bankeng deposit. (a) Inclusions of monazite, zircon, thorite,
814 and ilmenite in quartz. (b) Monazite replacing apatite. (c) A pseudomorph of bastnäsite-(Ce)
815 probably after a feldspar grain. (d) An inclusion of zircon in an apatite grain. (e) and (f)
816 Backscattered (BSE) images of other common LREE minerals in the parent granitoids. (e)
817 Allanite-(Ce) and quartz replacing K-feldspar at the Anxi deposit. (f) Inclusions of titanite and
818 allanite-(Ce) in biotite at the Nanqiao deposit. Abbreviations: Aln: allanite-(Ce), Ap: apatite,
819 Bst: bastnäsite-(Ce), Bt: biotite, Chl: chlorite, Ilm: ilmenite, Kfs: K-feldspar, Mnz: monazite,
820 Qtz: quartz, Tht: thorite, Ttn: titanite, Zrn: zircon.

821

822 **Figure 4**. Upper continental crust (UCC)-normalized REE profiles of the clay-adsorbed
823 fraction and water samples from (a) the Zudong deposit (Li et al., 2019) and (b) the footslope
824 profile of the Bankeng deposit (Li et al., 2020). The REE profiles of the ridgetop and upslope

Li, M. Y. H., Kwong, H. T., Williams-Jones, A. E., and Zhou, M.-F., 2021,
The thermodynamics of rare earth element liberation, mobilization and supergene enrichment during groundwater-regolith interaction:
Geochimica et Cosmochimica Acta.

825 regolith are also included for comparison. Note that the REE concentrations of all water
826 samples are multiplied by 10 for illustrative purposes.
827
828 **Figure 5**. Proportions of REE species in (a) aquifer groundwater and (b) regolith water of the
829 Zudong deposit. (c) – (f) Proportions of REE species in regolith water after dilution of the
830 bicarbonate content to (c) 25 mg/L, (d) 20 mg/L, (e) 15 mg/L, and (f) 10 mg/L.
831
832 **Figure 6**. Average proportion of REE species in the regolith groundwater from the Bankeng
833 deposit. (b) is an enlargement of part of (a) showing the proportions between 0 and 10%.
834

Li, M. Y. H., Kwong, H. T., Williams-Jones, A. E., and Zhou, M.-F., 2021,
The thermodynamics of rare earth element liberation, mobilization and supergene enrichment during groundwater-regolith interaction:
Geochimica et Cosmochimica Acta.

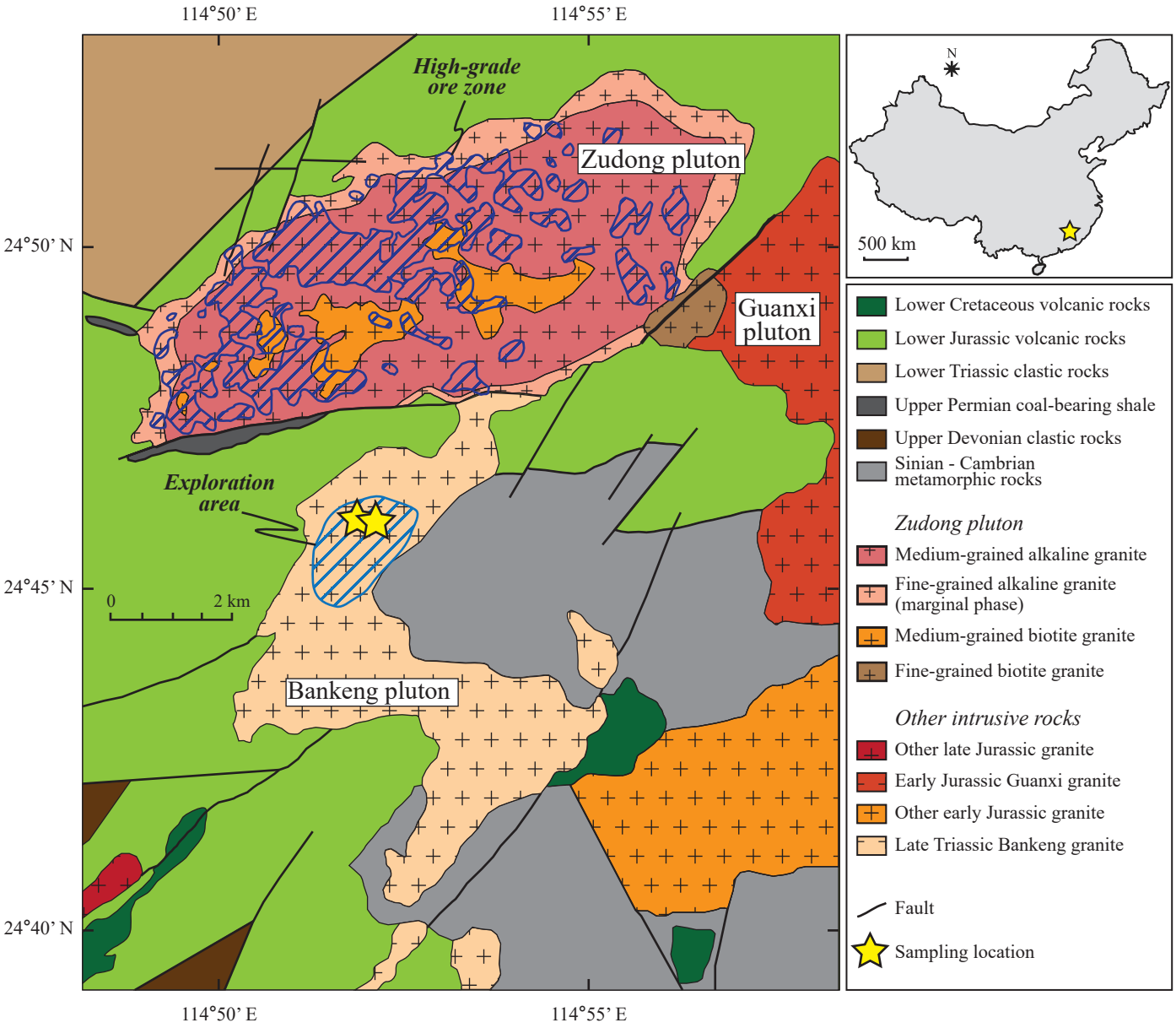

Figure 1

Li, M. Y. H., Kwong, H. T., Williams-Jones, A. E., and Zhou, M.-F., 2021,
The thermodynamics of rare earth element liberation, mobilization and supergene enrichment during groundwater-regolith interaction:
Geochimica et Cosmochimica Acta.

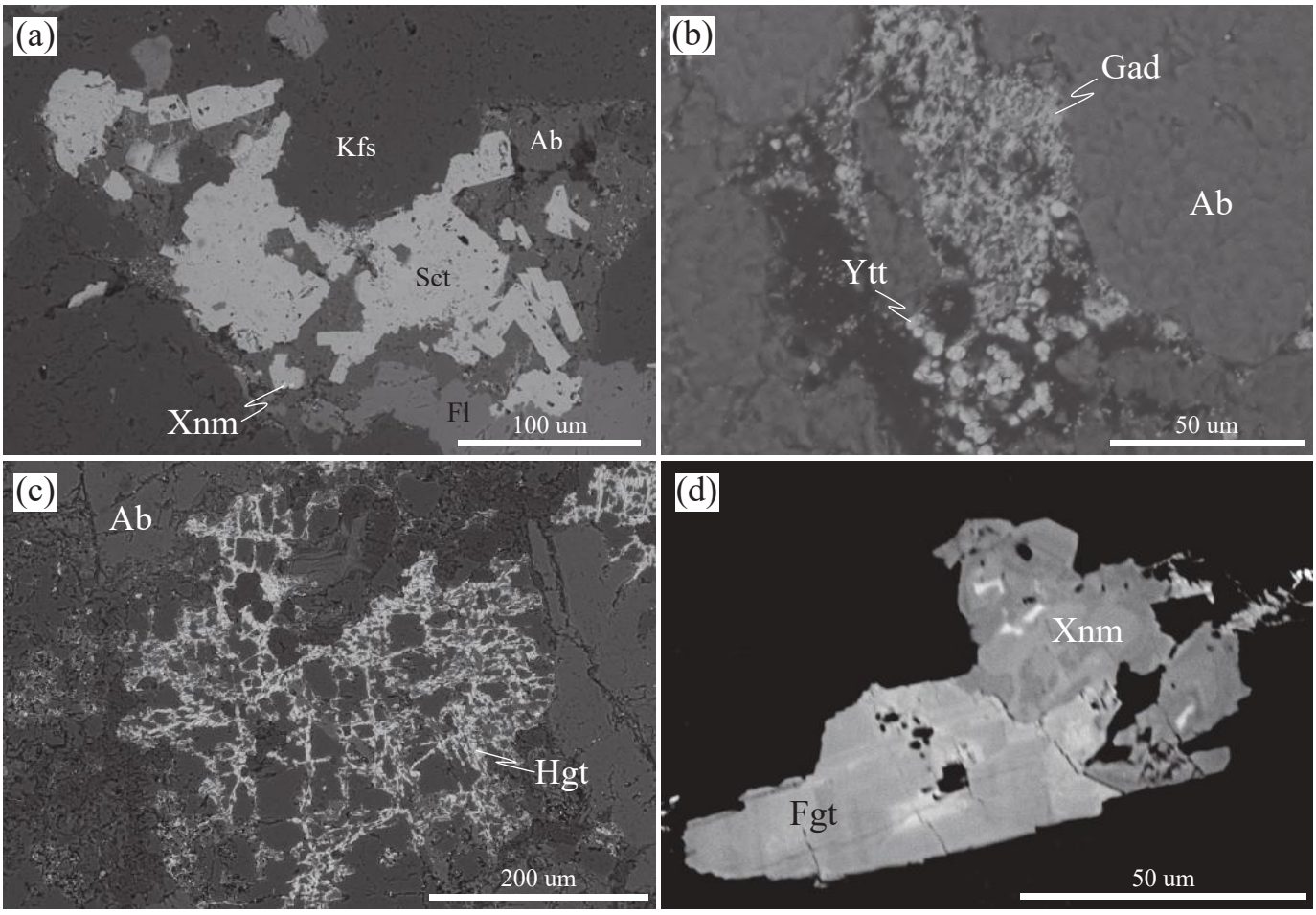

Figure 2

Li, M. Y. H., Kwong, H. T., Williams-Jones, A. E., and Zhou, M.-F., 2021,
The thermodynamics of rare earth element liberation, mobilization and supergene enrichment during groundwater-regolith interaction:
Geochimica et Cosmochimica Acta.

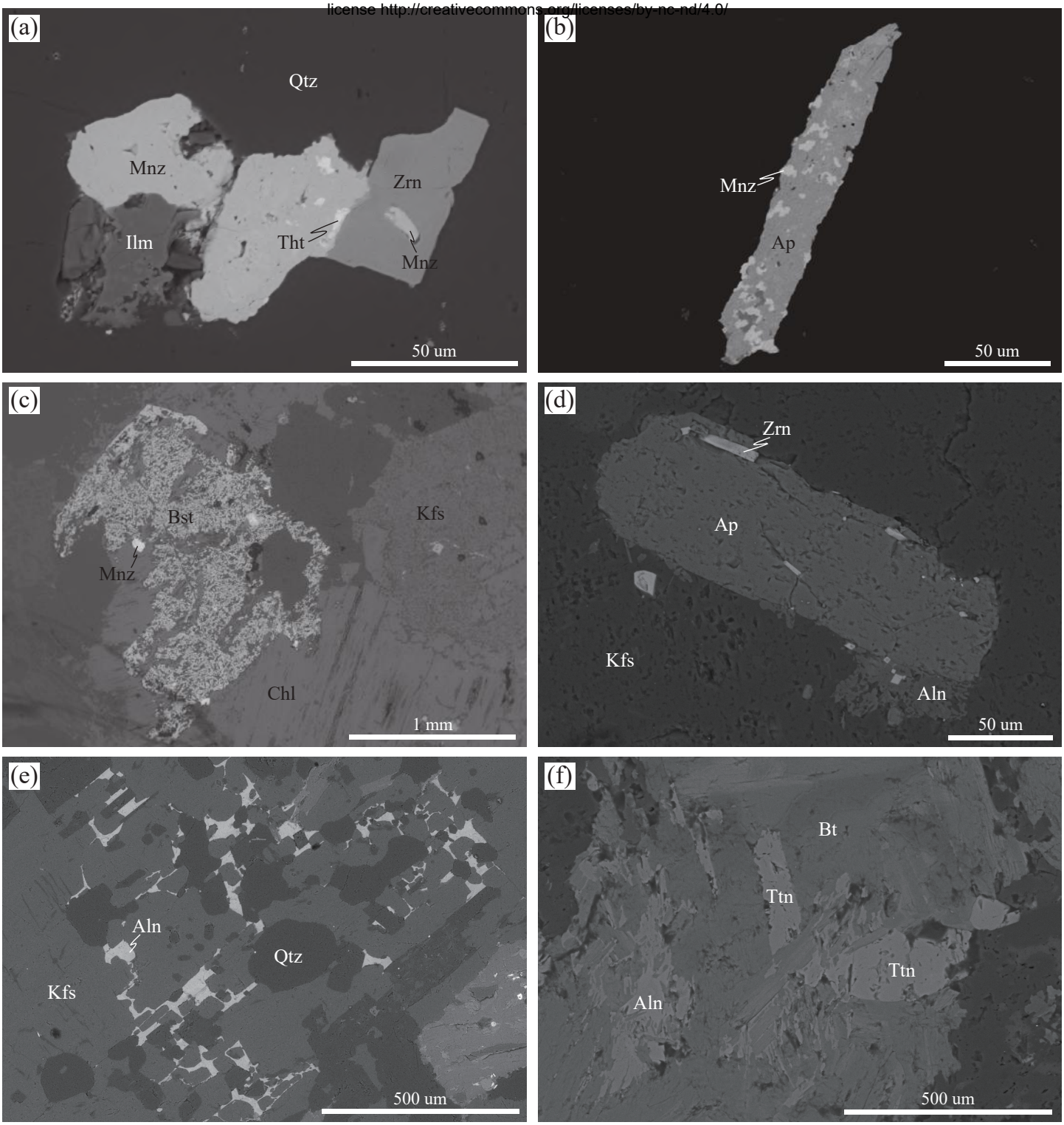

Figure 3

Li, M. Y. H., Kwong, H. T., Williams-Jones, A. E., and Zhou, M.-F., 2021,
The thermodynamics of rare earth element liberation, mobilization and supergene enrichment during groundwater-regolith interaction:
Geochimica et Cosmochimica Acta.

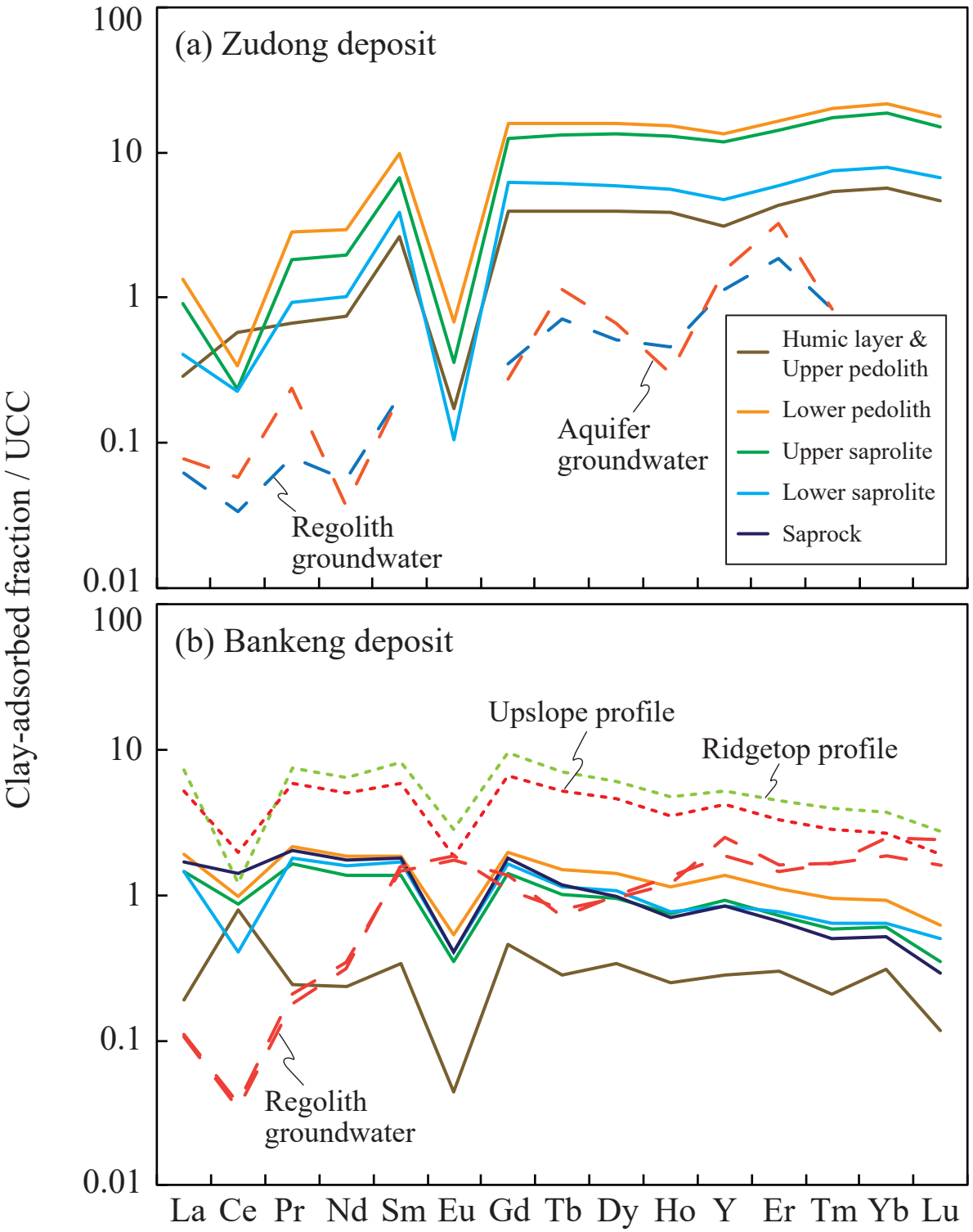

Figure 4

Li, M. Y. H., Kwong, H. T., Williams-Jones, A. E., and Zhou, M.-F., 2021,
The thermodynamics of rare earth element liberation, mobilization and supergene enrichment during groundwater-regolith interaction:
Geochimica et Cosmochimica Acta.

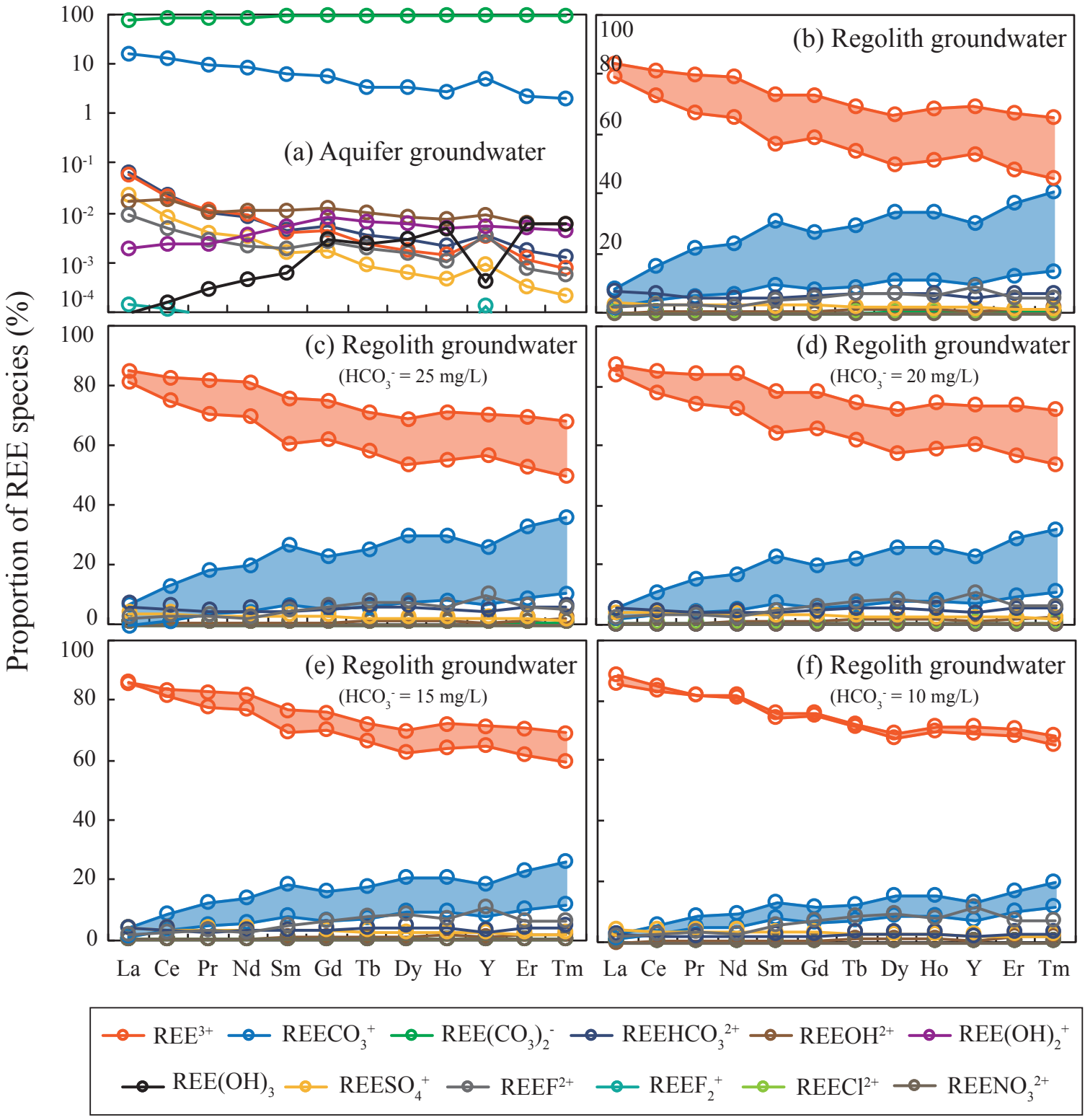

Figure 5

Li, M. Y. H., Kwong, H. T., Williams-Jones, A. E., and Zhou, M.-F., 2021,
The thermodynamics of rare earth element liberation, mobilization and supergene enrichment during groundwater-regolith interaction:
Geochimica et Cosmochimica Acta.

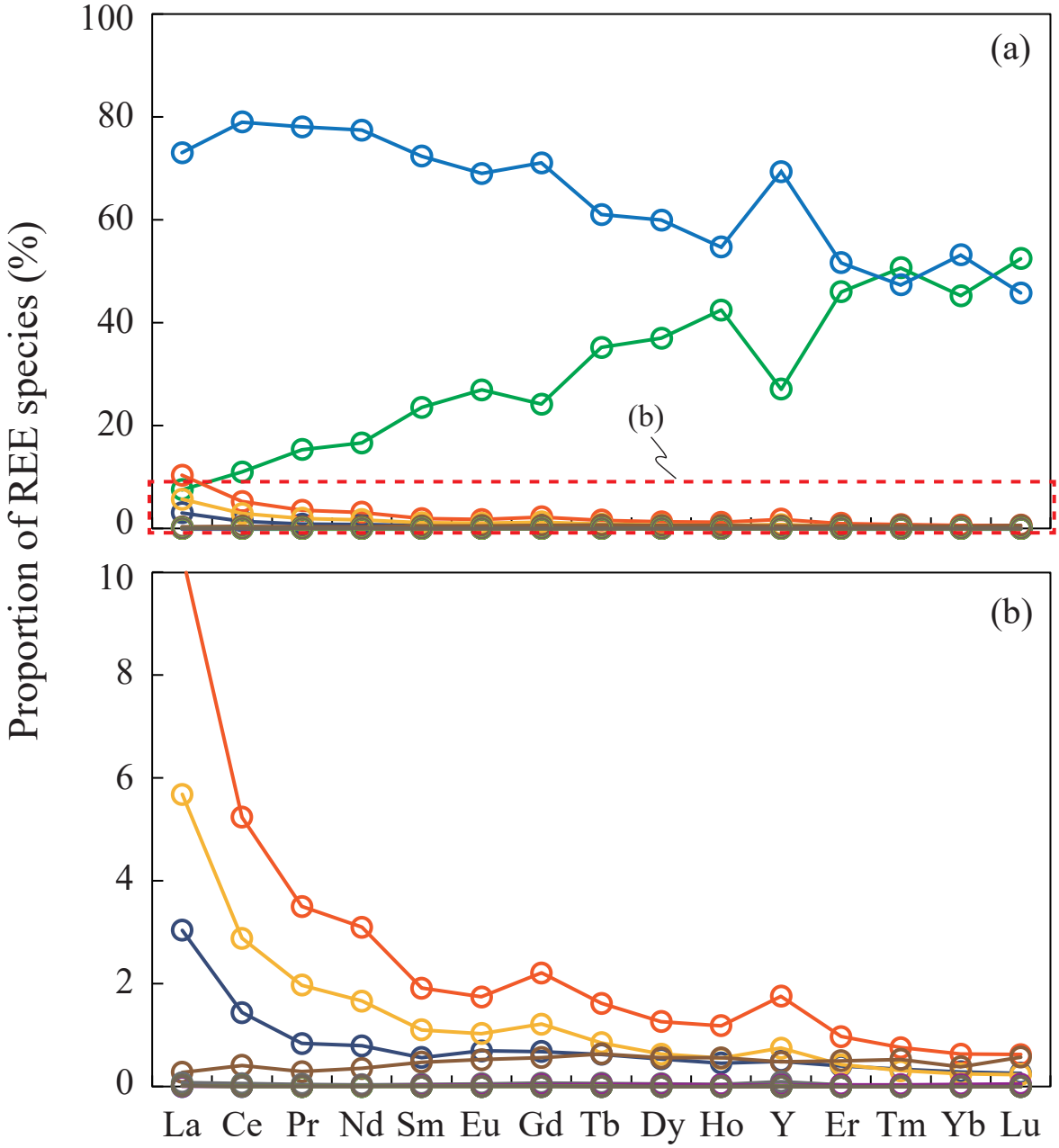

Figure 6

Li, M. Y. H., Kwong, H. T., Williams-Jones, A. E., and Zhou, M.-F., 2021,
The thermodynamics of rare earth element liberation, mobilization and supergene enrichment during groundwater-regolith interaction:
Geochimica et Cosmochimica Acta.

Table 1. Change in Gibbs free energy, equilibrium constant, and chemical quotients of dissolution reactions for common parental REE minerals

Mineral	Reaction formula	$\Delta G^{\circ}_{298.15K}$ (KJ mol^{-1})	log K	log Q_1	log Q_2	log Q_3	log Q_4
Bastnäsite-(Y)	$Y(CO_3)F + H^+ = Y^{3+} + HCO_3^- + F^-$	22.7 ± 14.3	-4.0 ± 2.5	-10.7 ± 0.2	-9.9 ± 0.2	-9.6 ± 0.2	-10.1 ± 0.2
Synchysite-(Y)	$CaY(CO_3)_2F + 2H^+ = Y^{3+} + Ca^{2+} + 2HCO_3^- + F^-$	-7.6 ± 19.2	1.3 ± 3.4	-13.2 ± 0.4	-11.8 ± 0.4	-7.7 ± 0.3	-8.3 ± 0.3
Gadolinite-(Y)	$Y_2FeBe_2Si_2O_{10} + 12H^+ = 2Y^{3+} + Fe^{2+} + 2H_4SiO_4 + 2Be^{2+} + 2H_2O$	-166.9 ± 34.2	29.2 ± 6.0	6.6 ± 0.8	13.5 ± 1.7	34.7 ± 4.4	40.5 ± 5.1
Hingganite-(Y)	$Y_2Be_2(SiO_4)_2(OH)_2 + 10H^+ = 2Y^{3+} + 2Be^{2+} + 2H_4SiO_4 + 2H_2O$	-101.8 ± 34.0	17.8 ± 6.0	15.8 ± 1.7	21.5 ± 2.3	37.7 ± 4.0	32.1 ± 3.4
Yttrialite-(Y)	$Y_2Si_2O_7 + 6H^+ + H_2O = 2Y^{3+} + 2H_4SiO_4$	-156.9 ± 31.7	27.5 ± 5.6	9.2 ± 0.6	12.5 ± 0.8	18.7 ± 1.2	17.3 ± 1.2
Parisite-(Ce)	$CaCe_2(CO_3)_3F_2 + 3H^+ = 2Ce^{3+} + Ca^{2+} + 3HCO_3^- + 2F^-$	342.1 ± 33.3	-59.9 ± 5.8	-26.3 ± 1.4	-23.9 ± 1.2	-17.9 ± 0.9	-19.6 ± 1.0
Synchysite-(Ce)	$CaCe(CO_3)_2F + 2H^+ = Ce^{3+} + Ca^{2+} + 2HCO_3^- + F^-$	14.8 ± 20.0	-2.5 ± 3.4	-14.4 ± 0.5	-12.9 ± 0.4	-8.0 ± 0.3	-8.9 ± 0.3
Bastnäsite-(Ce)[1]	$Ce(CO_3)F + H^+ = Ce^{3+} + HCO_3^- + F^-$	164.9 ± 15.1	-28.9 ± 2.7	-11.9 ± 0.2	-11.0 ± 0.2	-9.9 ± 0.2	-10.7 ± 0.2
Bastnäsite-(Ce)[2]	$Ce(CO_3)F + H^+ = Ce^{3+} + HCO_3^- + F^-$	44.7 ± 14.9	-7.8 ± 2.6	-11.9 ± 0.2	-11.0 ± 0.2	-9.9 ± 0.2	-10.7 ± 0.2
Chevkinite-(Ce)	$Ce_4Fe^{II}Fe^{III}{}_2Ti_2(Si_2O_7)_2O_8 + 20H^+ = 4Ce^{3+} + Fe^{2+} + 2Fe^{3+} + 2TiO_2\ (ant) + 4H_4SiO_4 + 2H_2O$	-480.6 ± 99.3	84.2 ± 17.4	-3.25 ± 0.7	8.51 ± 1.8	44.1 ± 9.3	54.1 ± 11.4
Allanite-(Ce)	$CaCe(Al_2Fe)(SiO_4)_3(OH) + 13H^+ = Ca^{2+} + Ce^{3+} + 2Al^{3+} + Fe^{2+} + 3H_4SiO_4 + H_2O$	-387.0 ± 47.6	67.8 ± 8.3	9.2 ± 1.3	16.6 ± 2.3	21.9 ± 3.0	37.9 ± 5.2
Titanite	$CaTiSiO_5 + 2H^+ + H_2O = Ca^{2+} + TiO_2\ (ant) + H_4SiO_4$	-50.3 ± 14.7	8.8 ± 2.6	2.5 ± 0.1	3.6 ± 0.1	8.7 ± 0.2	8.1 ± 0.2
Eudialyte	$Na_{15}Ca_6Fe_3Zr_3Si(Si_{25}O_{72})(OH)_5 + 45H^+ + 27H_2O = 15Na^+ + 6Ca^{2+} + 3Fe^{2+} + 3Zr^{4+} + 26H_4SiO_4$	-1010.5 ± 448.9	177.0 ± 78.6	-0.3 ± 0.2	26.7 ± 14.6	≈80 ± 44	≈120 ± 66
Apatite	$Ca_5(PO4)_3F + 9H^+ = 5Ca^{2+} + 3H_3PO_4 + F^-$	16.4 ± 44.3	-2.9 ± 7.8	-14.1 ± 1.5	-8.3 ± 0.9	15.3 ± 1.7	12.2 ± 1.3
Monazite-(Ce)	$CePO_4 + 3H^+ = Ce^{3+} + H_3PO_4$	31.1 ± 13.4	-5.5 ± 2.4	-4.5 ± 0.2	-2.7 ± 0.1	1.2 ± 0.1	0.2 ± 0.1
Xenotime-(Y)	$YPO_4 + 3H^+ = Y^{3+} + H_3PO_4$	44.4 ± 17.0	-7.8 ± 3.0	-3.3 ± 0.1	-1.62 ± 0.1	1.5 ± 0.1	0.8 ± 0.1
Fergusonite-(La)	$LaNbO_4 + 2H^+ = La^{3+} + NbO_3^- + H_2O$	89.3 ± 23.0	-15.6 ± 4.0	-8.8 ± 0.2	-7.6 ± 0.2	-6.0 ± 0.2	-5.6 ± 0.1
Fergusonite-(Y)	$YNbO_4 + 2H^+ = Y^{3+} + NbO_3^- + H_2O$	125.2 ± 23.3	-21.9 ± 4.1	-7.6 ± 0.2	-6.5 ± 0.2	-5.9 ± 0.1	-5.5 ± 0.1
Loparite-(Ce)	$(Na,Ce)(Nb,Fe^{III})O_6 + 6H^+ = Na^+ + Ce^{3+} + Fe^{3+} + NbO_3^- + 3H_2O$	-153.7 ± 51.1	26.9 ± 9.0	-10.9 ± 0.7	-7.4 ± 0.5	5.7 ± 0.4	5.0 ± 0.3
Zircon	$ZrSiO_4 + 4H^+ = Zr^{4+} + H_4SiO_4$	55.0 ± 53.9	-9.6 ± 2.6	8.0 ± 0.3	10.4 ± 0.4	20.4 ± 0.9	16.1 ± 0.7

Remarks:
1. Chemical quotients of reaction (Q) are calculated using regolith groundwater from Zudong at pH of 5.4 for Q_1, the same groundwater at pH of 6.0 for Q_2, aquifer groundwater from Zudong for Q_3, and averaged regolith groundwater from Bankeng for Q_4
2. "[1]": Data from Gysi and Williams-Jones (2015); "[2]": Data from Al-Nafai et al. (2019).

Li, M. Y. H., Kwong, H. T., Williams-Jones, A. E., and Zhou, M.-F., 2021,
The thermodynamics of rare earth element liberation, mobilization and supergene enrichment during groundwater-regolith interaction: Geochimica et Cosmochimica Acta.

Table 2. Change in Gibbs free energy, equilibrium constant, and chemical quotients of dissolution reactions for common parental REE minerals with the involvement of bicarbonate ion

Mineral	Reaction formula	$\Delta G^{\circ}_{298.15K}$ (KJ mol^{-1})	log K	log Q_1	log Q_2	log Q_3	log Q_4
Bastnäsite-(Y)	$Y(CO_3)F + H^+ = YCO_3^+ + HF$	20.9 ± 16.9	-3.7 ± 3.0	-10.4 ± 0.2	-9.9 ± 0.2	-9.2 ± 0.2	-9.3 ± 0.2
Synchysite-(Y)	$CaY(CO_3)_2F + 2H^+ = YCO_3^+ + Ca^{2+} + HCO_3^- + HF$	-9.4 ± 19.5	1.6 ± 3.4	-12.8 ± 0.4	-11.7 ± 0.3	-7.3 ± 0.2	-7.5 ± 0.2
Gadolinite-(Y)	$Y_2FeBe_2Si_2O_{10} + 10H^+ + 2HCO_3^- = 2YCO_3^+ + Fe^{2+} + 2H_4SiO_4 + 2Be^{2+} + 2H_2O$	-136.6 ± 41.8	24.0 ± 7.3	1.0 ± 0.1	7.9 ± 0.9	29.1 ± 3.2	35.7 ± 3.9
Hingganite-(Y)	$Y_2Be_2(SiO_4)_2(OH)_2 + 8H^+ + 2HCO_3^- = 2YCO_3^+ + 2Be^{2+} + 2H_4SiO_4 + 2H_2O$	-71.5 ± 41.6	12.5 ± 7.3	10.2 ± 0.9	15.9 ± 1.4	32.1 ± 2.9	27.4 ± 2.5
Yttrialite-(Y)	$Y_2Si_2O_7 + 4H^+ + 2HCO_3^- + H_2O = 2YCO_3^+ + 2H_4SiO_4$	-126.3 ± 38.5	22.1 ± 6.8	3.5 ± 0.2	6.8 ± 0.4	13.1 ± 0.7	12.6 ± 0.7
Parisite-(Ce)	$CaCe_2(CO_3)_3F_2 + 2H^+ = 2CeCO_3^+ + Ca^{2+} + CO_3^{2-} + 2HF$	402.3 ± 35.9	-70.5 ± 6.3	-36.7 ± 1.4	-34.9 ± 1.3	-28.1 ± 1.1	-29.8 ± 1.1
Synchysite-(Ce)	$CaCe(CO_3)_2F + 2H^+ = CeCO_3^+ + Ca^{2+} + HCO_3^- + HF$	15.1 ± 19.9	-2.6 ± 3.5	-14.4 ± 0.4	-13.2 ± 0.4	-8.0 ± 0.2	-8.9 ± 0.3
Bastnäsite-(Ce)[1]	$Ce(CO_3)F + H^+ = CeCO_3^+ + HF$	165.5 ± 17.5	-28.9 ± 3.1	-12.0 ± 0.2	-11.4 ± 0.2	-10.0 ± 0.2	-10.7 ± 0.2
Bastnäsite-(Ce)[2]	$Ce(CO_3)F + H^+ = CeCO_3^+ + HF$	45.3 ± 17.3	-7.9 ± 3.0	-12.0 ± 0.2	-11.4 ± 0.2	-10.0 ± 0.2	-10.7 ± 0.2
Chevkinite-(Ce)	$Ce_4Fe^{II}Fe^{III}_2Ti_2(Si_2O_7)_2O_8 + 16H^+ + 4HCO_3^- = 4CeCO_3^+ + Fe^{2+} + 2Fe^{3+} + 2TiO_2\,(ant) + 4H_4SiO_4 + 2H_2O$	-409.9 ± 102.1	71.9 ± 17.9	-16.3 ± 2.9	-4.5 ± 0.8	31.2 ± 5.5	41.2 ± 7.3
Allanite-(Ce)	$CaCe(Al_2Fe)(SiO_4)_3(OH) + 12H^+ + HCO_3^- = Ca^{2+} + CeCO_3^+ + 2Al^{3+} + Fe^{2+} + 3H_4SiO_4 + H_2O$	-364.2 ± 49.0	67.8 ± 8.3	6.0 ± 0.8	13.4 ± 1.7	18.7 ± 2.4	34.6 ± 4.4
Monazite-(Ce)	$CePO_4 + 2H^+ + HCO_3^- = CeCO_3^+ + H_3PO_4$	49.8 ± 17.9	-8.7 ± 3.1	-7.7 ± 0.2	-6.0 ± 0.2	-2.0 ± 0.1	-3.0 ± 0.1
Xenotime-(Y)	$YPO_4 + 2H^+ + HCO_3^- = YCO_3^+ + H_3PO_4$	60.7 ± 20.1	-10.6 ± 3.6	-6.1 ± 0.2	-4.4 ± 0.1	-1.3 ± 0.0	-1.6 ± 0.0
Fergusonite-(La)	$LaNbO_4 + H^+ + HCO_3^- = LaCO_3^+ + NbO_3^- + H_2O$	109.7 ± 25.9	-19.2 ± 4.5	-12.4 ± 0.3	-11.2 ± 0.2	-9.5 ± 0.2	-9.2 ± 0.2
Fergusonite-(Y)	$YNbO_4 + H^+ + HCO_3^- = YCO_3^+ + NbO_3^- + H_2O$	141.4 ± 26.2	-25.0 ± 4.6	-10.4 ± 0.2	-9.3 ± 0.2	-8.7 ± 0.2	-7.9 ± 0.2
Loparite-(Ce)	$(Na,Ce)(Nb,Fe^{III})O_6 + 5H^+ + HCO_3^- = Na^+ + CeCO_3^+ + Fe^{3+} + NbO_3^- + 3H_2O$	-135.1 ± 52.5	23.6 ± 9.2	-14.2 ± 0.8	-10.7 ± 0.6	2.5 ± 0.1	1.7 ± 0.1

Remarks:
1. Chemical quotients of reaction (Q) are calculated using regolith groundwater from Zudong at pH of 5.4 for Q_1, the same groundwater at pH of 6.0 for Q_2, aquifer groundwater from Zudong for Q_3, and averaged regolith groundwater from Bankeng for Q_4.
2. "[1]": Data from Gysi and Williams-Jones (2015); "[2]": Data from Al-Nafai et al. (2019).

Li, M. Y. H., Kwong, H. T., Williams-Jones, A. E., and Zhou, M.-F., 2021,
The thermodynamics of rare earth element liberation, mobilization and supergene enrichment during groundwater-regolith interaction: Geochimica et Cosmochimica Acta.

Table 3. Chemistry of the groundwater samples from the Zudong and Bankeng deposits

	Zudong deposit[1]		Bankeng deposit	
	Regolith water	Aquifer groundwater	BK19-1	BK19-2
pH	5.4 - 6.0	8.5	7.49	7.39
Concentration in mg/L				
NH_4^+	b.dl.	0.14	b.dl.	b.dl.
SO_4^{2-}	1.44	33.4	46.0	45.9
CO_3^{2-}	b.dl.	22.8	-	-
HCO_3^-	31.26	573.2	148	143
NO_3^-	b.dl.	0.35	48.0	48.0
F^-	0.41	4.3	0.19	0.20
Cl^-	3.3	10.2	22.3	22.4
Al	0.17	b.dl.	b.dl.	b.dl.
Fe	b.dl.	b.dl.	b.dl.	b.dl.
Mg	0.98	1.88	9.20	9.24
Ca	1.33	2.41	69.7	70.0
Na	3.85	227.6	19.6	19.6
K	1.37	14.1	35.4	35.2
TOC	-	-	1.20	1.51
Ionic strength (M)	0.001	0.012	0.008	0.008
Ionic imbalance (%)	28.6 - 28.8	3.8	11.5	12.5
Concentration in µg/L				
Li	-	-	3.29	3.31
Be	-	-	0.56	0.34
Al	-	-	2.47	7.73
Si	-	-	9383	8904
P	-	-	53.7	67.5
Sc	-	-	0.88	0.95
Ti	-	-	1.45	1.38
V	-	-	1.65	1.71
Cr	-	-	0.64	0.70
Mn	-	-	0.72	1.19
Fe	-	-	106	159
Co	-	-	0.14	0.15
Ni	-	-	0.94	1.01
Zn	-	-	1.09	1.13
Ga	-	-	0.02	0.01
Ge	-	-	0.08	0.04
As	-	-	0.72	0.79
Rb	-	-	61.0	60.2
Sr	-	-	118	123
Y	2.4	3.25	3.89	5.20
Zr	-	-	0.08	0.05
Nb	-	-	0.04	0.01
Cd	-	-	0.05	0.07
Sn	-	-	0.06	b.dl.
Sb	-	-	0.08	0.08
Cs	-	-	1.27	1.25
Ba	-	-	109	119
La	0.2	0.25	0.35	0.34
Ce	0.22	0.38	0.24	0.22
Pr	0.05	0.15	0.13	0.11
Nd	0.15	0.1	0.92	0.83
Sm	0.1	0.1	0.68	0.73
Eu	b.dl.	b.dl.	0.17	0.18
Gd	0.14	0.11	0.54	0.43
Tb	0.05	0.08	0.05	0.06
Dy	0.2	0.26	0.39	0.37
Ho	0.038	0.025	0.11	0.10
Er	0.43	0.75	0.33	0.37
Tm	0.025	0.025	0.05	0.05
Yb	b.dl.	b.dl.	0.37	0.49
Lu	b.dl.	b.dl.	0.05	0.07
Hf	-	-	0.03	0.01
Ta	-	-	0.02	0.00
W	-	-	0.69	0.39
Pb	-	-	b.dl.	b.dl.
Th	-	-	0.03	0.01
U	-	-	3.02	2.82
REE	4.00	5.48	8.28	9.55

"b.dl.": below detection limit, "-": not detected

[1]: Data from Wu (1988)

Li, M. Y. H., Kwong, H. T., Williams-Jones, A. E., and Zhou, M.-F., 2021,
The thermodynamics of rare earth element liberation, mobilization and supergene enrichment during groundwater-regolith interaction:
Geochimica et Cosmochimica Acta.

The thermodynamics of rare earth element liberation, mobilization and supergene enrichment during groundwater-regolith interaction

Martin Yan Hei Li[1], Hiu Tung Kwong[1], Anthony E. Williams-Jones[1, 2], Mei-Fu Zhou[1]

1 Department of Earth Sciences, The University of Hong Kong, Pokfulam Road, Hong Kong

2 Department of Earth and Planetary Sciences, McGill University, Montréal,

Québec H3A 0E8, Canada

Supplementary materials

Table S1. The Gibbs free energy of formation (gi) of the polyhedral units used to estimate the Gibbs free energy of REE minerals

Table S2. The ΔG_f of the species used in the calculation

Table S3. Aqueous speciation constants for REE with different ligands

Table S4. Saturation indices of selected phases in the groundwater samples

Table S5. Summary of the REE concentrations and anomalies of different soil horizons from the Zudong deposit

Table S6. Summary of the REE concentrations and anomalies of different soil horizons from the Bankeng deposit

Figure S1. Proportion of REE species in (a) aquifer groundwater and (b - f) regolith groundwater of the Zudong deposit using the stability constants for carbonate species from Liu and Byrne (1998)

Figure S2. Averaged proportion of REE species in the regolith groundwater from the Bankeng deposit using the stability constants for carbonate species from Liu and Byrne (1998)

Li, M. Y. H., Kwong, H. T., Williams-Jones, A. E., and Zhou, M.-F., 2021,
The thermodynamics of rare earth element liberation, mobilization and supergene enrichment during groundwater-regolith interaction:
Geochimica et Cosmochimica Acta.

Table S1. The Gibbs free energy of formation (g_i) of the polyhedral units used to estimate the Gibbs free energy of REE minerals

Polyhedral unit	g_i (KJ mol^{-1})	SD (KJ mol^{-1})	References
Al_2O_3	-1594.52	15.3	(Chermak and Rimstidt, 1989)
Na_2O	-672.50	26.0	(Chermak and Rimstidt, 1989)
CaO	-669.13	5.9	(Chermak and Rimstidt, 1989)
FeO	-266.29	6.8	(Chermak and Rimstidt, 1989)
Fe_2O_3	-776.07	33.0	(Chermak and Rimstidt, 1989)
SiO_2	-853.95	4.6	(Chermak and Rimstidt, 1989)
H_2O	-239.91	5.7	(Chermak and Rimstidt, 1989)
TiO_2	-972.02	35.7	(Van Hinsberg et al., 2005)
BeO	-612.68	3.5	(Van Hinsberg et al., 2005)
Ce_2O_3	-1709.6	10.7	(Navrotsky et al., 2015)
Y_2O_3	-1884.1	6.2	(Navrotsky et al., 2015)
Nb_2O_5	-1768.2	88.4*	(Hill et al., 1971)
ZrO_2	-1039.7	52.0*	(Stull and Prophet, 1971)
CO_2	-440.4	0.4	(La Iglesia and Felix, 1994)

*: Standard deviation (SD) is estimated as 5% of the g_i of the corresponding polyhedral unit.

Table S2. The G_f of the species used in the calculation

	G_f (KJ mol^{-1})	SD (KJ mol^{-1})	References
Na^+	-261.88	2.6**	(Shock and Helgeson, 1988)
Ca^{2+}	-552.79	5.5**	(Shock and Helgeson, 1988)
Be^{2+}	-349.36	3.5**	(Shock and Helgeson, 1988)
Fe^{2+}	-91.546	0.9**	(Shock and Helgeson, 1988)
Fe^{3+}	-17.062	0.2**	(Shock and Helgeson, 1988)
Al^{3+}	-482.74	4.8**	(Shock and Helgeson, 1988)
La^{3+}	-686.18	6.9**	(Shock and Helgeson, 1988)
Ce^{3+}	-676.13	6.7**	(Shock and Helgeson, 1988)
Y^{3+}	-685.34	6.9**	(Shock and Helgeson, 1988)
Zr^{4+}	-557.60	5.6**	(Shock et al., 1997)
NbO_3^-	-950.19	9.5**	(Shock et al., 1997)
F^-	-281.75	2.8**	(Shock and Helgeson, 1988)
CO_3^{2-}	-527.98	5.3**	(Shock and Helgeson, 1988)
HCO_3^-	-586.94	5.7**	(Shock and Helgeson, 1988)
$LaCO_3^+$	-1252.6	12.5**	This study
$CeCO_3^+$	-1244.4	12.4**	This study
YCO_3^+	-1256.0	12.6**	This study
HF	-299.84	3.0**	(Shvarov, 1999)
H_2O	-237.25	2.4**	(Shvarov, 1999)
H_4SiO_4	-1308.7	13.1**	(Shvarov, 1999)
H_3PO_4	-1142.7	11.4**	(Shvarov, 1999)
TiO_2 (anatase)	-883.20	2.1	(Robie and Hemingway, 1995)
Bastnäsite-(Y)	-1576.7	10.8	This study
Synchysite-(Y)	-2686.2	12.3	This study
Gadolinite-(Y)	-5083.7	14.8	This study
Hingganite-(Y)	-5057.3	14.3	This study
Yttrialite-(Y)	-3592.0	11.1	This study

Parisite-(Ce)	-4571.5	24.0	(Gysi and Williams-Jones, 2015)
Synchysite-(Ce)	-2699.0	13.1	This study
Bastnäsite-(Ce)	-1709.7	12.0	(Gysi and Williams-Jones, 2015)
Bastnäsite-(Ce)	-1589.5	11.7	(Al-Nafai et al., 2019)
Chevkinite-(Ce)	-9821.4	83.8	This study
Allanite-(Ce)	-6066.5	23.3	This study
Titanite	-2456.2	2.0	(Manon et al., 2008)
Eudialyte	-35779	280	This study
Fluoroapatite	-6508.1	5.0	(Robie, 1978)
Monazite-(Ce)	-1849.9	2.3	(Popa and Konings, 2006)
Xenotime-(Y)	-1872.4	10.5	(Navrotsky et al., 2015)
Fergusonite-(La)	-1962.8	19.6**	(Nikiforova et al., 2019; Reznitskii, 2001)
Fergusonite-(Y)	-1997.9	20.0**	This study
Loparite-(Ce)	-2463.2	49.2	This study
Zircon	-1920.2	4.4	(Schuiling et al., 1976)

**: Standard deviation (SD) is estimated as 1% of the G_f of the corresponding species.

Table S3. Aqueous speciation constants for REE with different ligands

Equation	$\log {}_{L}\beta_n$	La	Ce	Pr	Nd	Sm	Eu	Gd	Tb	Dy	Ho	Y	Er	Tm	Yb	Lu	Ref
$REE^{3+} + H_2O = REE(OH)^{2+} + H^+$	$\log {}_{OH}\beta^*_1$	-8.81	-8.34	-8.32	-8.18	-7.84	-7.76	-7.83	-7.64	-7.59	-7.56	-7.8	-7.52	-7.39	-7.45	-7.27	[1]
$REE^{3+} + 2H_2O = REE(OH)_2^+ + 2H^+$	$\log {}_{OH}\beta^*_2$	-18.1	-17.6	-17.3	-17.0	-16.5	-16.4	-16.4	-16.2	-16.1	-16.1	-16.4	-16.0	-15.9	-15.7	-15.7	[2]
$REE^{3+} + 3H_2O = REE(OH)_3 + 3H^+$	$\log {}_{OH}\beta^*_3$	-27.9	-27.2	-26.6	-26.4	-25.9	-25.4	-25.3	-25.1	-24.8	-24.6	-26.0	-24.4	-24.2	-23.9	-23.9	[2]
$REE^{3+} + CO_3^{2-} = REECO_3^+$	$\log {}_{CO3}\beta_1$	6.73	7.06	7.23	7.28	7.46	7.48	7.39	7.46	7.56	7.55	7.48	7.61	7.68	7.81	7.75	[3]
$REE^{3+} + 2CO_3^{2-} = REE(CO_3)_2^-$	$\log {}_{CO3}\beta_2$	11.3	11.76	12.08	12.17	12.53	12.63	12.48	12.78	12.91	13.00	12.63	13.12	13.27	13.30	13.37	[3]
$REE^{3+} + CO_3^{2-} = REECO_3^+$	$\log {}_{CO3}\beta_1$	6.98	7.31	7.48	7.53	7.71	7.73	7.64	7.71	7.81	7.80	7.73	7.86	7.93	7.06	8.00	[4]*
$REE^{3+} + 2CO_3^{2-} = REE(CO_3)_2^-$	$\log {}_{CO3}\beta_2$	11.86	12.32	12.63	12.73	13.09	13.19	13.04	13.34	13.47	13.56	13.19	13.68	13.83	13.86	13.93	[4]*
$REE^{3+} + HCO_3^- = REEHCO_3^{2+}$	$\log {}_{HCO3}\beta_1$	2.34	2.31	2.25	2.28	2.34	2.47	2.36	2.46	2.5	2.46	2.32	2.49	2.52	2.53	2.49	[3]
$REE^{3+} + NO_3^- = REENO_3^{2+}$	$\log {}_{NO3}\beta_1$	0.58	0.69	0.69	0.79	0.78	0.83	0.47	0.51	0.15	0.25	-	0.15	0.2	0.25	0.56	[5]
$REE^{3+} + F^- = REEF^{2+}$	$\log {}_{F}\beta_1$	3.11	3.29	3.35	3.29	3.61	3.72	3.71	3.83	3.88	3.78	3.97	3.77	3.77	3.84	3.74	[6]
$REE^{3+} + 2F^- = REEF_2^+$	$\log {}_{F}\beta_2$	5.16	5.48	5.66	5.66	5.99	6.11	6.07	6.24	6.29	5.98	6.35	5.96	6.09	6.31	6.31	[6]
$REE^{3+} + SO_4^{2-} = REESO_4^+$	$\log {}_{SO4}\beta_1$	3.61	3.61	3.62	3.6	3.63	3.64	3.61	3.59	3.57	3.54	3.5	3.51	3.48	3.46	3.44	[7]
$REE^{3+} + Cl^- = REECl_2^+$	$\log {}_{Cl}\beta_1$	0.65	0.65	0.65	0.65	0.65	0.65	0.65	0.65	0.65	0.65	0.65	0.65	0.65	0.65	0.65	[8]

*: Constants used for sensitivity check

Ref: [1]: Klugness and Byrne (2000); [2]: Lee and Byrne (1992); [3]: Luo and Byrne (2004); [4]: Liu and Byrne (1998); [5]: Millero (1992); [6]: Luo and Millero (2004); [7]: Schijf and Byrne (2004); [8]: Luo and Byrne (2001).

Li, M. Y. H., Kwong, H. T., Williams-Jones, A. E., and Zhou, M.-F., 2021,
The thermodynamics of rare earth element liberation, mobilization and supergene enrichment during groundwater-regolith interaction:
Geochimica et Cosmochimica Acta.

Table S4. Saturation indices of selected phases in the groundwater samples

	Zudong deposit		Bankeng deposit	
Phase	Regolith groundwater	Aquifer groundwater	BK19-1	BK19-2
Amorphous $Al(OH)_3$	-2.59 – -0.96	-	-2.63	-2.12
Ca-Montmorillonite	/	/	-0.72	0.34
Calcite	-4.28 – -3.68	0.09	0.04	-0.08
Dolomite	-8.34 – -7.15	0.44	-0.46	-0.68
Amorphous $Fe(OH)_3$	-	-	1.74	1.86
Gibbsite	0.10 – 1.73	-	0.06	0.57
Goethite	-	-	7.63	7.75
Hematite	-	-	17.26	17.52
Illite	/	/	-0.90	0.07
Kaolinite	/	/	1.30	2.27
Talc	/	/	-2.49	-3.18

'-': Below detection limit

'/': Not applicable

Li, M. Y. H., Kwong, H. T., Williams-Jones, A. E., and Zhou, M.-F., 2021,
The thermodynamics of rare earth element liberation, mobilization and supergene enrichment during groundwater-regolith interaction:
Geochimica et Cosmochimica Acta.

Table S5. Summary of the REE concentrations and anomalies of different soil horizons from the Zudong deposit

	Humic layer & Upper pedolith			Lower pedolith			Upper saprolite		
	Bulk	Clay-sorbed	Fe oxide-sorbed	Bulk	Clay-sorbed	Fe oxide-sorbed	Bulk	Clay-sorbed	Fe oxide-sorbed
REE	376	211	9.7	1048	736	24.4	899	589	18.7
LREE	95	72	3.6	204	163	6.7	124	109	4.6
HREE	281	140	6.1	843	573	17.7	774	480	14.1
$(La/Yb)_N$	0.46	0.61	1.2	0.67	0.82	1.1	0.45	0.74	1.16
Y/Ho	25.3	18.8	21.0	26.3	21.9	21.7	27.7	22.1	23.0
Ce/Ce*	1.41	2.99	0.74	0.29	0.24	0.18	0.31	0.19	0.20
Sm/Sm*	1.56	1.58	1.58	1.50	1.45	1.52	1.47	1.38	1.47
Gd/Gd*	1.16	1.23	1.18	1.19	1.27	1.17	1.25	1.33	1.20
Y/Y*	0.93	0.70	0.81	1.01	0.84	0.78	1.05	0.84	0.87
Yb/Yb*	1.05	1.15	1.16	1.04	1.13	1.09	1.04	1.15	1.03

Li, M. Y. H., Kwong, H. T., Williams-Jones, A. E., and Zhou, M.-F., 2021,
The thermodynamics of rare earth element liberation, mobilization and supergene enrichment during groundwater-regolith interaction:
Geochimica et Cosmochimica Acta.

Table S5. Summary of the REE concentrations and anomalies of different soil horizons from the Zudong deposit (Con't)

	Lower saprolite			Parent granite
	Bulk	Clay-sorbed	Fe oxide-sorbed	Bulk
REE	598	272	10.1	332
LREE	90	66	2.7	57
HREE	508	206	7.4	274
$(La/Yb)_N$	0.41	0.71	0.90	0.41
Y/Ho	27.8	21.6	22.5	31.9
Ce/Ce*	0.5	0.56	0.44	0.84
Sm/Sm*	1.46	1.44	1.47	1.39
Gd/Gd*	1.28	1.32	1.17	1.24
Y/Y*	1.05	0.83	0.86	1.19
Yb/Yb*	1.04	1.12	1.11	1.02

All concentrations are in ppm

All data obtained from Li et al. (2019); clay-sorbed and Fe oxide-sorbed fractions were determined by chemical extraction with ammonium sulfate and hydroxylammonium chloride, respecitvely.

Calculation of elemental anomalies:

$Ce/Ce^* = Ce_{UCC}/\sqrt{La_{UCC} \times Nd_{UCC}}$; $Sm/Sm^* = Sm_{UCC}/\sqrt{Nd_{UCC} \times Gd_{UCC}}$; $Gd/Gd^* = Gd_{UCC}/\sqrt{Sm_{UCC} \times Tb_{UCC}}$;

$Y/Y^* = Y_{UCC}/\sqrt{Ho_{UCC} \times Er_{UCC}}$; $Yb/Yb^* = Yb_{UCC}/\sqrt{Tm_{UCC} \times Lu_{UCC}}$

Li, M. Y. H., Kwong, H. T., Williams-Jones, A. E., and Zhou, M.-F., 2021,
The thermodynamics of rare earth element liberation, mobilization and supergene enrichment during groundwater-regolith interaction:
Geochimica et Cosmochimica Acta.

Table S6. Summary of the REE concentrations and anomalies of different soil horizons from the Bankeng deposit

	Footslope profile								
	Humic layer & Upper pedolith			Lower pedolith			Upper saprolite		
	Bulk	Clay-sorbed	Fe oxide-sorbed	Bulk	Clay-sorbed	Fe oxide-sorbed	Bulk	Clay-sorbed	Fe oxide-sorbed
REE	202	78	19.9	436	246	80.2	332	191	55.5
LREE	148	65	18.4	338	188	76.0	253	151	53.1
HREE	54	12	1.0	98	58	2.6	79	40	1.5
$(La/Yb)_N$	3.87	5.5	7.5	14.1	23.7	24.1	12.8	28.2	31.1
Y/Ho	29.4	26.4	23.8	29.7	30.4	27.9	27.9	31.6	28.9
Ce/Ce*	2.86	7.02	12.5	1.04	0.51	7.59	0.98	0.60	7.17
Sm/Sm*	0.96	1.08	0.83	0.98	0.96	0.85	0.99	0.97	0.88
Gd/Gd*	1.18	1.73	1.79	1.11	1.19	1.73	1.07	1.21	1.66
Y/Y*	1.09	0.91	0.91	1.14	1.22	1.11	1.08	1.26	1.13
Yb/Yb*	1.02	1.68	0.81	1.02	1.21	1.07	1.04	1.33	1.20

Li, M. Y. H., Kwong, H. T., Williams-Jones, A. E., and Zhou, M.-F., 2021,
The thermodynamics of rare earth element liberation, mobilization and supergene enrichment during groundwater-regolith interaction:
Geochimica et Cosmochimica Acta.

Table S6. Summary of the REE concentrations and anomalies of different soil horizons from the Bankeng deposit (Con't)

	Footslope profile					Ridgetop profile			Upslope profile			Parent granite
	Lower saprolite			Saprock								
	Bulk	Clay-sorbed	Fe oxide-sorbed	Bulk	Clay-sorbed	Bulk	Clay-sorbed	Fe oxide-sorbed	Bulk	Clay-sorbed	Fe oxide-sorbed	Bulk
REE	386	170	173	359	249	963	779	95.0	839	655	62.4	292
LREE	318	128	169	271	207	715	536	86.7	595	473	52.2	235
HREE	68	42	3.2	88	42	248	242	5.7	244	183	5.9	58
$(La/Yb)_N$	16.3	26.8	31.3	15.2	39.4	30.4	22.9	52.7	17.8	22.5	25.1	19.5
Y/Ho	25.3	27.8	20.3	27.1	30.3	24.3	28.0	23.1	26.8	30.2	28.1	28.2
Ce/Ce*	1.33	0.23	11.6	0.79	0.78	0.25	0.16	1.26	0.43	0.36	1.33	0.91
Sm/Sm*	1.06	1.03	0.98	1.03	1.00	1.09	1.04	1.07	1.06	1.01	1.09	1.04
Gd/Gd*	0.99	1.21	1.33	1.08	1.25	1.13	1.26	1.22	1.12	1.20	1.20	1.04
Y/Y*	1.01	1.11	0.81	1.05	1.23	1.00	1.14	0.91	1.07	1.23	1.13	1.12
Yb/Yb*	1.00	1.12	1.07	1.04	1.42	0.99	1.12	1.17	1.07	1.17	1.11	1.02

All concentrations are in ppm

All data obtained from Li et al. (2020); clay-sorbed and Fe oxide-sorbed fractions were determined by chemical extraction with ammonium sulfate and hydroxylammonium chloride, respecitvely.

Calculation of elemental anomalies:

$Ce/Ce^* = Ce_{UCC}/\sqrt{La_{UCC} \times Nd_{UCC}}$; $Sm/Sm^* = Sm_{UCC}/\sqrt{Nd_{UCC} \times Gd_{UCC}}$; $Gd/Gd^* = Gd_{UCC}/\sqrt{Sm_{UCC} \times Tb_{UCC}}$;

$Y/Y^* = Y_{UCC}/\sqrt{Ho_{UCC} \times Er_{UCC}}$; $Yb/Yb^* = Yb_{UCC}/\sqrt{Tm_{UCC} \times Lu_{UCC}}$

Li, M. Y. H., Kwong, H. T., Williams-Jones, A. E., and Zhou, M.-F., 2021,
The thermodynamics of rare earth element liberation, mobilization and supergene enrichment during groundwater-regolith interaction:
Geochimica et Cosmochimica Acta.

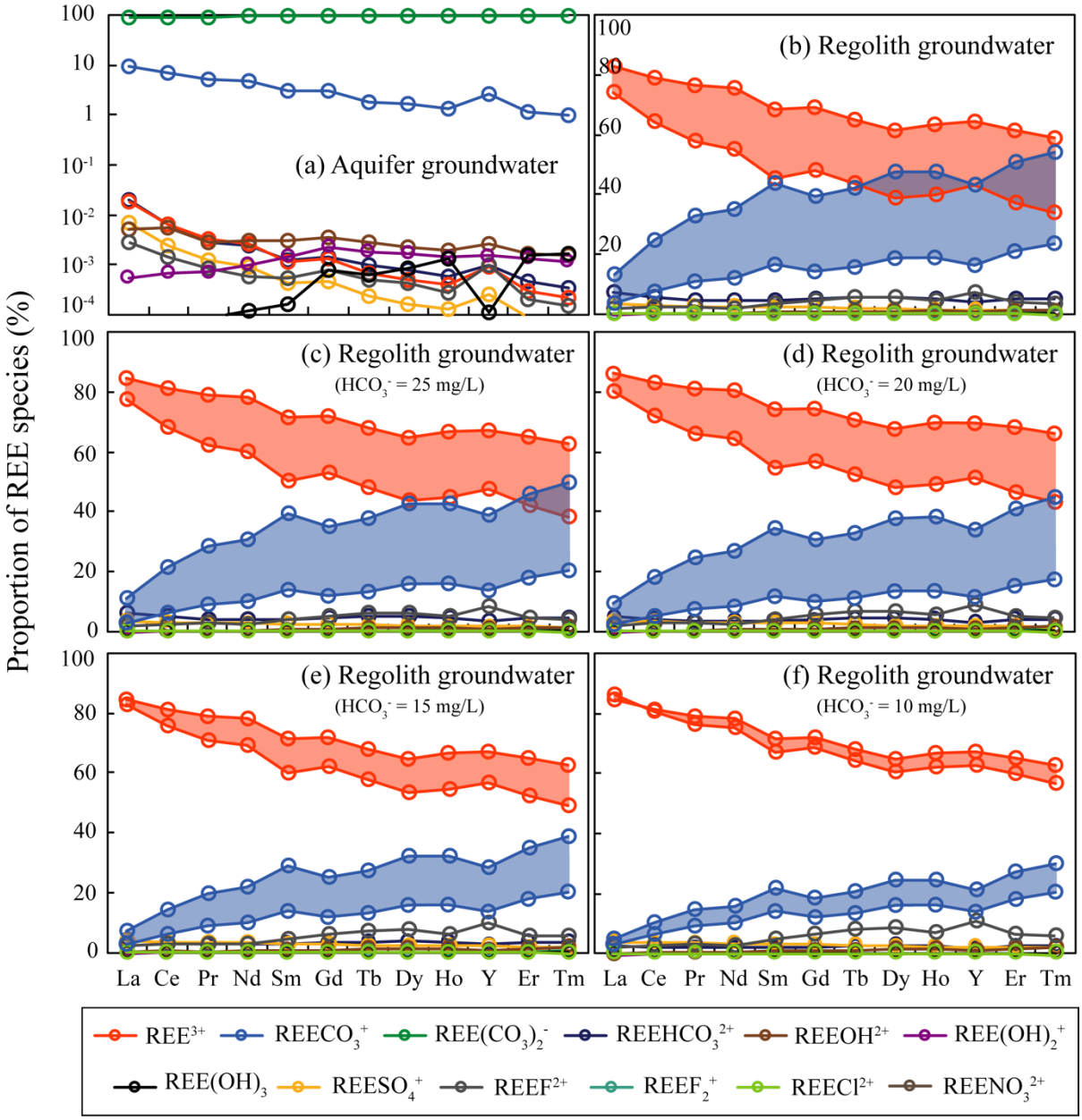

Figure S1. Proportion of REE species in (a) aquifer groundwater and (b - f) regolith groundwater of the Zudong deposit using the stability constants for carbonate species from Liu and Byrne (1998). (c) – (f) Simulation of the spring water with diluted bicarbonate contents as (c) 25 mg/L, (d) 20 mg/L, (e) 15 mg/L, and (f) 10 mg/L.

Li, M. Y. H., Kwong, H. T., Williams-Jones, A. E., and Zhou, M.-F., 2021,
The thermodynamics of rare earth element liberation, mobilization and supergene enrichment during groundwater-regolith interaction:
Geochimica et Cosmochimica Acta.

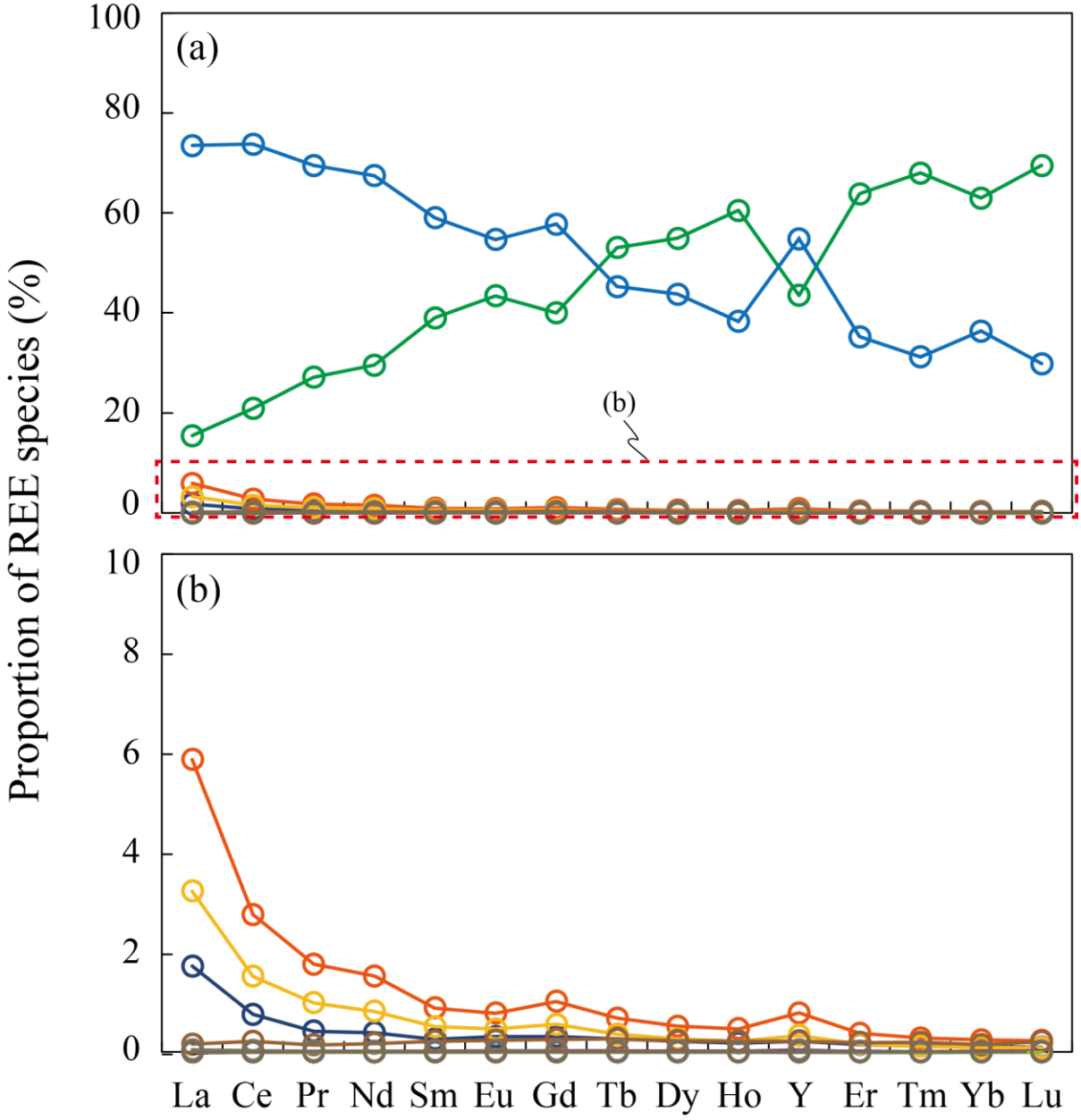

Figure S2. Averaged proportion of REE species in the regolith groundwater from the Bankeng deposit using the stability constants for carbonate species from Liu and Byrne (1998)

Li, M. Y. H., Kwong, H. T., Williams-Jones, A. E., and Zhou, M.-F., 2021,
The thermodynamics of rare earth element liberation, mobilization and supergene enrichment during groundwater-regolith interaction:
Geochimica et Cosmochimica Acta.

References

Al-Nafai, I., Kim, H. and Osseo-Asare, K. (2019) Estimation of the standard free energy of formation of bastnasite, REFCO 3. Mining, Metallurgy & Exploration 36, 227-233.

Chermak, J.A. and Rimstidt, J.D. (1989) Estimating the thermodynamic properties (ΔG^{0f} and ΔH^{0f}) of silicate minerals at 298 K from the sum of polyhedral contributions. American Mineralogist 74, 1023-1031.

Gysi, A.P. and Williams-Jones, A.E. (2015) The thermodynamic properties of bastnäsite-(Ce) and parisite-(Ce). Chemical Geology 392, 87-101.

Hill, J.O., Worsley, I.G. and Hepler, L.G. (1971) Thermochemistry and oxidation potentials of vanadium, niobium, and tantalum. Chemical Reviews 71, 127-137.

Klungness, G.D. and Byrne, R.H. (2000) Comparative hydrolysis behavior of the rare earths and yttrium: the influence of temperature and ionic strength. Polyhedron 19, 99-107.

La Iglesia, A. and Felix, J. (1994) Estimation of thermodynamic properties of mineral carbonates at high and low temperatures from the sum of polyhedral contributions. Geochimica et Cosmochimica Acta 58, 3983-3991.

Lee, J.H. and Byrne, R.H. (1992) Examination of comparative rare earth element complexation behavior using linear free-energy relationships. Geochimica et Cosmochimica Acta 56, 1127-1137.

Li, M.Y.H., Zhou, M.-F. and Williams-Jones, A.E. (2019) The genesis of regolith-hosted heavy rare earth element deposits: Insights from the world-class Zudong deposit in Jiangxi Province, South China. Economic Geology 114, 541-568.

Li, M.Y.H., Zhou, M.-F. and Williams-Jones, A.E. (2020) Controls on the dynamics of rare earth elements during sub-tropical hillslope processes and formation of regolith-hosted deposits. Economic Geology 115, 1097-1118.

Liu, X. and Byrne, R.H. (1998) Comprehensive Investigation of Yttrium and Rare Earth Element Complexation by Carbonate Ions Using ICP–Mass Spectrometry. Journal of Solution Chemistry 27, 803-815.

Luo, Y.-R. and Byrne, R.H. (2001) Yttrium and rare earth element complexation by chloride ions at 25 C. Journal of Solution Chemistry 30, 837-845.

Luo, Y.-R. and Byrne, R.H. (2004) Carbonate complexation of yttrium and the rare earth elements in natural waters. Geochimica et Cosmochimica Acta 68, 691-699.

Luo, Y. and Millero, F.J. (2004) Effects of temperature and ionic strength on the stabilities of the first and second fluoride complexes of yttrium and the rare earth elements. Geochimica et Cosmochimica Acta 68, 4301-4308.

Manon, M., Dachs, E. and Essene, E. (2008) Low T heat capacity measurements and new entropy data for titanite (sphene): implications for thermobarometry of high-pressure rocks. Contributions to Mineralogy and Petrology 156, 709.

Millero, F.J. (1992) Stability constants for the formation of rare earth-inorganic complexes as a function of ionic strength. Geochimica et Cosmochimica Acta 56, 3123-3132.

Navrotsky, A., Lee, W., Mielewczyk-Gryn, A., Ushakov, S.V., Anderko, A., Wu, H. and Riman, R.E. (2015) Thermodynamics of solid phases containing rare earth oxides. The Journal of Chemical Thermodynamics 88, 126-141.

Nikiforova, G., Khoroshilov, A., Tyurin, A., Gurevich, V. and Gavrichev, K. (2019) Heat capacity and thermodynamic properties of lanthanum orthoniobate. The Journal of Chemical Thermodynamics 132, 44-53.

Popa, K. and Konings, R. (2006) High-temperature heat capacities of EuPO4 and SmPO4 synthetic monazites. Thermochimica Acta 445, 49-52.

Reznitskii, L.A. (2001) Formation enthalpies of Nb (IV, V) oxide compounds. Inorganic Materials 37, 491-495.

Robie, R. (1978) Thermodynamic properties of minerals and related substances at 298.15 K and 1 bar (105 Pascal) pressure and at higher temperatures. US Geological Survery Bulletin 1452, 298-310.

Robie, R.A. and Hemingway, B.S. (1995) Thermodynamic properties of minerals and related substances at 298.15 K and 1 bar (10^5 pascals) pressure and at higher temperatures.

Schijf, J. and Byrne, R.H. (2004) Determination of $SO_4\beta_1$ for yttrium and the rare earth elements at I= 0.66 m and t= 25° C—implications for YREE solution speciation in sulfate-rich waters1. Geochimica et Cosmochimica Acta 68, 2825-2837.

Schuiling, R.D., Vergouwen, L. and Rijst, H. (1976) Gibbs energies of formation of zircon ($ZrSiO_4$), thorite ($ThSiO_4$), and phenacite (Be_2SiO_4). American Mineralogist 61, 166-168.

Shock, E.L. and Helgeson, H.C. (1988) Calculation of the thermodynamic and transport properties of aqueous species at high pressures and temperatures: Correlation algorithms for ionic species and equation of state predictions to 5 kb and 1000 C. Geochimica et Cosmochimica Acta 52, 2009-2036.

Shock, E.L., Sassani, D.C., Willis, M. and Sverjensky, D.A. (1997) Inorganic species in geologic fluids: correlations among standard molal thermodynamic properties of aqueous ions and hydroxide complexes. Geochimica et Cosmochimica Acta 61, 907-950.

Shvarov, Y.V. (1999) Algorithmization of the numeric equilibrium modeling of dynamic geochemical processes. Geochemistry International 37, 571-576.

Stull, D.R. and Prophet, H. (1971) JANAF thermochemical tables. National Standard Reference Data System.

Van Hinsberg, V., Vriend, S. and Schumacher, J. (2005) A new method to calculate end-member thermodynamic properties of minerals from their constituent polyhedra I: enthalpy, entropy and molar volume. Journal of Metamorphic Geology 23, 165-179.